


New 1,2,3-triazole linked ciprofloxacin-chalcones induce DNA damage by inhibiting human topoisomerase I & II and tubulin polymerization

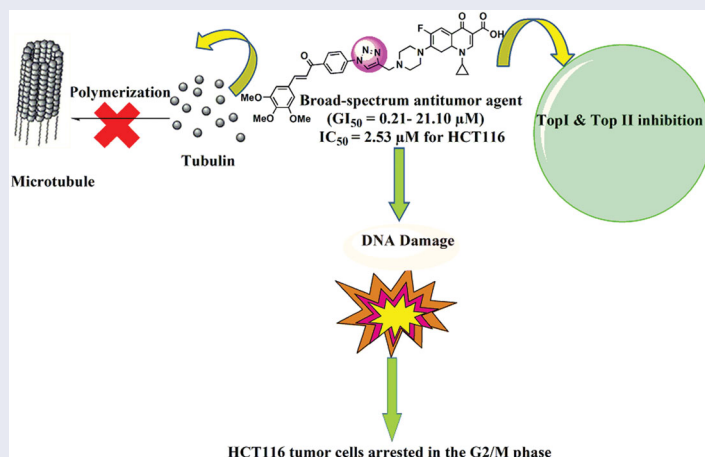
Hamada H. H. Mohammed^{a,b,*}, Amer Ali Abd El-Hafeez^{c,d,*}, Kareem Ebeid^{e,f,g}, Aml I. Mekkawy^{f,h}, Mohammed A. S. Abourehabⁱ, Emad I. Wafa^f, Suhaila O. Alhaj-Suliman^f, Aliasger K. Salem^{f,j}, Pradipta Ghosh^{c,k,l,m}, Gamal El-Din A. Abu-Rahma^{a,n}, Alaa M. Hayallah^{o,p} and Samar H. Abbas^a 

^aDepartment of Medicinal Chemistry, Faculty of Pharmacy, Minia University, Minia, Egypt; ^bDepartment of Pharmaceutical Chemistry, Faculty of Pharmacy, Sohag University, Sohag, Egypt; ^cDepartment of Cellular and Molecular Medicine, University of California San Diego, La Jolla, CA, USA; ^dCancer Biology Department, Pharmacology and Experimental Oncology Unit, National Cancer Institute, Cairo University, Cairo, Egypt; ^eDepartment of Pharmaceutics, Faculty of Pharmacy, Minia University, Minia, Egypt; ^fDepartment of Pharmaceutical Sciences and Experimental Therapeutics, College of Pharmacy, University of Iowa, Iowa City, IA, USA; ^gDepartment of Pharmaceutics, Faculty of Pharmacy and Pharmaceutical Manufacturing, Deraya University, New Minia City, Minia, Egypt; ^hDepartment of Pharmaceutics and Clinical Pharmacy, Faculty of Pharmacy, Sohag University, Sohag, Egypt; ⁱDepartment of Pharmaceutics, Faculty of Pharmacy, Umm Al Qura University, Makkah, Saudi Arabia; ^jHolden Comprehensive Cancer Center, University of Iowa, Iowa City, IA, USA; ^kDepartment of Medicine, University of California San Diego, La Jolla, CA, USA; ^lRebecca and John Moore Comprehensive Cancer Center, University of California San Diego, La Jolla, CA, USA; ^mVeterans Affairs Medical Center, La Jolla, CA, USA; ⁿDepartment of Pharmaceutical Chemistry, Faculty of Pharmacy, Deraya University, Minia, Egypt; ^oPharmaceutical Organic Chemistry Department, Faculty of Pharmacy, Assiut University, Assiut, Egypt; ^pPharmaceutical Chemistry Department, Faculty of Pharmacy, Sphinx University, New Assiut, Egypt

ABSTRACT

A series of novel 1,2,3-triazole-linked ciprofloxacin-chalcones **4a-j** were synthesised as potential anticancer agents. Hybrids **4a-j** exhibited remarkable anti-proliferative activity against colon cancer cells. Compounds **4a-j** displayed IC₅₀s ranged from 2.53–8.67 μM, 8.67–62.47 μM, and 4.19–24.37 μM for HCT116, HT29, and Caco-2 cells; respectively, whereas the doxorubicin, showed IC₅₀ values of 1.22, 0.88, and 4.15 μM. Compounds **4a**, **4b**, **4e**, **4i**, and **4j** were the most potent against HCT116 with IC₅₀ values of 3.57, 4.81, 4.32, 4.87, and 2.53 μM, respectively, compared to doxorubicin (IC₅₀ = 1.22 μM). Also, hybrids **4a**, **4b**, **4e**, **4i**, and **4j** exhibited remarkable inhibitory activities against topoisomerase I, II, and tubulin polymerisation. They increased the protein expression level of γH2AX, indicating DNA damage, and arrested HCT116 in G2/M phase, possibly through the ATR/CHK1/Cdc25C pathway. Thus, the novel ciprofloxacin hybrids could be exploited as potential leads for further investigation as novel anticancer medicines to fight colorectal carcinoma.

GRAPHICAL ABSTRACT








ARTICLE HISTORY


Received 24 February 2022
Revised 15 April 2022
Accepted 26 April 2022

KEYWORDS

Click synthesis;
ciprofloxacin; chalcone;
cytotoxicity; HCT116 cells;
topoisomerase I and II
inhibitors; tubulin
polymerisation inhibition;
DNA damage

CONTACT Samar H. Abbas  samar_hafez@mu.edu.eg; Gamal El-Din A Abu-Rahma  gamal.aborahama@mu.edu.eg  Department of Medicinal Chemistry, Faculty of Pharmacy, Minia University, Minia, Egypt; Aliasger K. Salem:  aliasger-salem@uiowa.edu  Department of Pharmaceutical Sciences and Experimental Therapeutics, College of Pharmacy, University of Iowa, Iowa City, IA, USA

*These authors have contributed equally to this work.

 Supplemental data for this article can be accessed [here](#).

© 2022 The Author(s). Published by Informa UK Limited, trading as Taylor & Francis Group.

This is an Open Access article distributed under the terms of the Creative Commons Attribution License (<http://creativecommons.org/licenses/by/4.0/>), which permits unrestricted use, distribution, and reproduction in any medium, provided the original work is properly cited.

1. Introduction

Cancer is a complicated pathological condition characterised by uncontrolled cell growth¹. As the 2nd leading cause of mortality, cancer accounts for 21% of annual deaths globally²⁻⁴. By 2040, the number of new cases is estimated to reach 29.4 million per year, compared to 18.1 million in 2018⁵. Colorectal Cancer (CRC) was the second most deadly cancer and the third most common malignancy in 2020, which caused 1.9 million incidence cases and 0.9 million deaths globally. The Predictable number of new CRC cases worldwide in 2040 will be 3.2 million cases⁶. Surgery, chemotherapy, and radiotherapy are currently available cancer treatment options⁷. Although single target chemotherapy achieves some therapeutic benefits, its use is limited by poor efficacy, serious toxic effects and the development of resistance^{8,9}. Two strategies for multi-target therapeutics are being used in preclinical or clinical practice to overcome such problems¹⁰. The first one is combination therapy; the clinical use of this approach is widely utilised for the treatment of various types of cancer. Still, some combinations may be limited due to undesirable drug-drug interactions¹¹. The second strategy is based on using smart hybrids or multi-target directed ligands (MTDLs). Two or more pharmacophore fragments are linked together to form a single molecule that can simultaneously modulate multiple oncoproteins^{12,13}. Thus, the use of multi-target directed ligands can improve efficacy, reduce serious adverse effects, and prevent the development of drug resistance^{14,15}. Understanding various molecular pathways utilised in the development and formation of tumours can aid in the discovery of novel antitumor agents¹⁶. Ciprofloxacin (CP) is a broad-spectrum antibacterial agent that acts by poisoning bacterial DNA gyrase (topoisomerase II) and topoisomerase IV^{17,18}, which are fundamental enzymes that substantially contribute to the process of DNA replication¹⁹⁻²¹. CP has recently gained considerable attention as an anti-proliferative agent^{21,22}. It was reported that poisoning topoisomerase II, arresting cell cycle arrest, and inducing apoptosis are the mechanisms responsible for the anti-proliferative activity of CP²³⁻²⁵. Accordingly, shifting the biological profile of CP from antibacterial to anticancer candidate appears to be possible due to its profound apoptotic and anti-proliferative potential²⁶. In this regard, the structural modifications required for

anticancer activity of CP have been clearly discussed^{1,27}. Bio-isosteric replacement of the carboxylic group at C-3 of CP with tetrazole heterocyclic ring markedly improves its anti-proliferative activity^{1,28}. Also, one key modification was carried out by substituting its *N*-4 piperazine heterocycle moiety with an aryl or heteroaryl bulky group^{1,27}. Introducing a substituent on the *N*-4-piperazinyl moiety of CP affects the physicochemical characteristics and/or significantly improves the anti-proliferative activity²⁹⁻³¹. The nature of the *N*-4-piperazinyl substituent remarkably affects the capacity of CP derivatives to suppress the activity of DNA topoisomerases³². In addition, the potential selectivity of CP derivatives to human topoisomerases was found to be significantly improved via modification of the *N*-4-piperazine heterocycle³¹. Consequently, several CP derivatives have been prepared, characterised, and widely explored for their antitumor properties^{33,34}. Recent studies have revealed that the presence of different chalcones on the *N*-4-piperazine moiety of CP gave rise to new CP hybrids with potent anti-proliferative activities targeting multiple oncoproteins (Figure 1)^{16,21}. Furthermore, the introduction of the aryl sulfamoyl group into the *N*-4 piperazine of CP gave rise to new fluoroquinolone derivatives with anticancer activity³⁵. Substitution of *N*-4 piperazine of CP with 4-chlorophenylcarbamoyl led to a new CP derivative with potent anti-proliferative activity against non-small cell lung cancer (Figure 1)³⁶. On the other hand, natural and synthetic chalcones represent a vital and central component of various compounds with diverse biological properties³⁷. Chalcone is a familiar scaffold in medicinal chemistry that is widely used for the development of a large number of molecules with potential anticancer activities^{38,39}. The anticancer potential of chalcone-containing compounds was attributed to apoptosis induction, angiogenesis inhibition, DNA damage, kinases inhibition, and tubulin inhibition^{40,41}. Chalcones have gained considerable attention from drug hunters due to their ease of synthesis, exploring novel scaffolds with potential biological activities^{42,43}.

Furthermore, 1,2,3-Triazoles are essential scaffolds in medicinal chemistry that are widely used in many drug-design protocols as bio-isosteres of ester, amide, and other heterocycles^{44,45}. Compounds containing 1,2,3-triazole heterocycle can form different non-covalent interactions such as hydrogen bonds, dipole-dipole bonds, hydrophobic interactions, and van der Waals forces

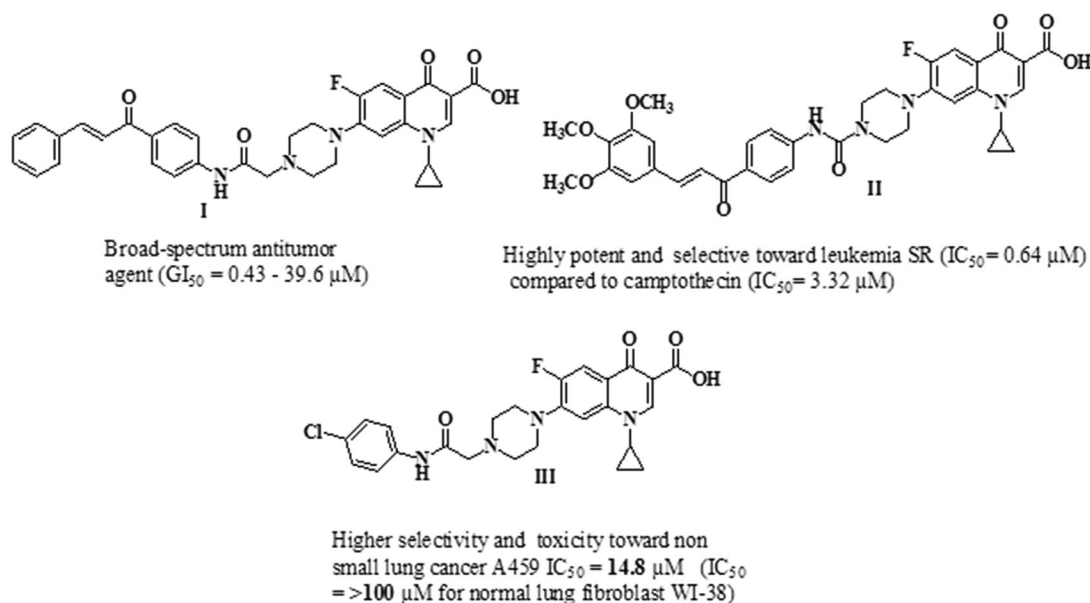


Figure 1. Chemical structures of several examples of some reported *N*-4 piperazinyl ciprofloxacin derivatives with anti-proliferative activities.

with various biological targets, thus they possess various biological effects (e.g., anticancer^{46–49}, antibacterial^{50,51}, antifungal^{52,53}, antiviral^{54,55}, antimalarial^{56,57}, and antitubercular^{58,59} activities). Additionally, 1,2,3-Triazole is a favourable basic unit in the finding of new anticancer agents, and some of its derivatives have now been in clinics or under clinical trials for combating against cancers⁴⁵. 1,2,3-Triazoles exhibited their anticancer effects via different modes of action. They exerted their anti-proliferative effects through Tubulin polymerisation inhibition or inhibition of some kinases such as epidermal growth factor receptor, c-Met Kinase, and vascular endothelial growth factor. They also caused inhibition of vital enzymes such as aromatase, tryptophan 2,3-dioxygenase, carbonic anhydrases, and thymidylate synthase⁶⁰. Also, many drugs have 1,2,3-triazole moiety, such as cefatrizine **IV**, seviteronel **V**, carboxyamidotriazole **VI**, and mubritinib **VII** entered active clinical trials in 2021 (Figure 2)⁶¹.

Moreover, several 1,2,3-triazole chalcone hybrids were reported as anticancer agents aiming for synergistic activity in the last decade. For example, 1,2,3-triazole-chalcone hybrid **VIII** exhibited nanomolar IC₅₀ values against six cancer cell lines, HCT-116 colon, RPMI-8226 leukaemia, MCF7 breast, SR leukaemia, M14 melanoma, and K-562 leukaemia cancer cell lines, and sensitive cell lines. It caused induction of apoptosis in a dose-dependent manner through activation of caspases 3, 7 & 9 and Bax/Bcl-2 ratio elevation⁶². Additionally, Chalcone/1,2,3-triazole hybrid **IX** was reported as an orally tubulin polymerisation inhibitor. Compound **IX** inhibited proliferation and migration in HepG2 cells growth in a dose-dependent manner⁶³. Furthermore, 1,2,3-triazole tethered chalcone hybrid **X** showed potent cytotoxic activity on MCF-7 cancer cell lines with IC₅₀ of 1.27 μM and 0.02 μM at 24 and 48 h; respectively⁶⁴ (Figure 3).

Inspired by the above-mentioned aspects, the purpose of our study was to develop a new series of 1,2,3-triazole linked CP-chalcone hybrids **4a–j** as possible multi-target-directed ligands with potential anti-proliferative activities. Their *in-vitro* cytotoxic activity was evaluated using National Cancer Institute (NCI) aganist59 cancer cell lines. Additionally, the IC₅₀s of the new CP derivatives **4a–j** against three different colon cancer cell lines (Caco-2, HT29, and HCT116) were determined using the MTT assay. Furthermore, as possible molecular targets, the ability of the most active hybrids to inhibit tubulin polymerisation and the catalytic activities of both topoisomerases I and topoisomerases II were examined. Also, the ability of the most promising hybrids to induce DNA double strand breaks and cell cycle arrest in HCT116 cancer cells in

addition to their effect on the protein expression levels of γH2AX was evaluated. Moreover, the docking studies of new hybrids were investigated at the TopI (**1T8I**) and Top II (**6ZY7**) active sites. To the best of our knowledge, this is the first report that gathers these three important pharmacophores; Ciprofloxacin, Chalcone and 1,2,3-triazole in one compact unit aiming for synergistic anti-cancer activity through acting on different molecular targets (Figure 4).

2. Results and discussion

2.1. Chemistry

Both new compounds and their intermediates were synthesised as drawn in Scheme 1. In particular, the intermediate 1-(4-azidophenyl)ethanone **1** was prepared following the previously published procedures^{65,66}. Chalcone derivatives **2a–j** were synthesised by condensation of 1-(4-azidophenyl)ethanone **1** with the appropriate aromatic aldehyde in ethanol in presence of sodium hydroxide^{65,66}. Compound **3** was prepared by alkylation of CP with propargyl bromide in dimethylformamide (DMF) in the presence of NaHCO₃⁶⁷. The final compounds **4a–j** were synthesised by coupling chalcone derivatives **2a–j** with CP derivative **3** in DMF using sodium ascorbate and copper sulphate as a catalyst. Structure elucidation of our target compounds was carried out via IR, ¹H NMR, ¹³C NMR, elemental analysis, and mass spectrometry. The IR spectra of compounds **4a**, **4e**, and **4i** as representative examples showed a broad stretching bands at 3200–3048 cm⁻¹ assigned to OH of the carboxylic group, in addition to three carbonyl stretching bands appeared at 1719–1715 cm⁻¹, 1658–1657 cm⁻¹, and 1625–1622 cm⁻¹ assigned to C=O of the carboxylic, carbonyl of the chalcone and the 4-keto functionality, respectively. The pattern of parent CP and chalcone scaffolds was confirmed by ¹H NMR. Chemical shifts (δ) at 1.19–1.35 ppm and 3.45–3.85 ppm (two multiplet signals) represent the protons of cyclopropyl and piperazine moieties, respectively. Also, aromatic protons (3) and carboxylic proton of CP appeared at δ=7.56–8.66 ppm and 15.05–15.17 ppm, respectively. The two chalcone protons appeared at δ=7.58–8.03 ppm. One characteristic singlet for the triazolyl *H* appeared at δ 8.83–8.93 ppm. Moreover, ¹³C NMR showed a characteristic signal at δ=186.77–188.90 ppm which corresponds to the carbonyl group of the chalcone scaffold.

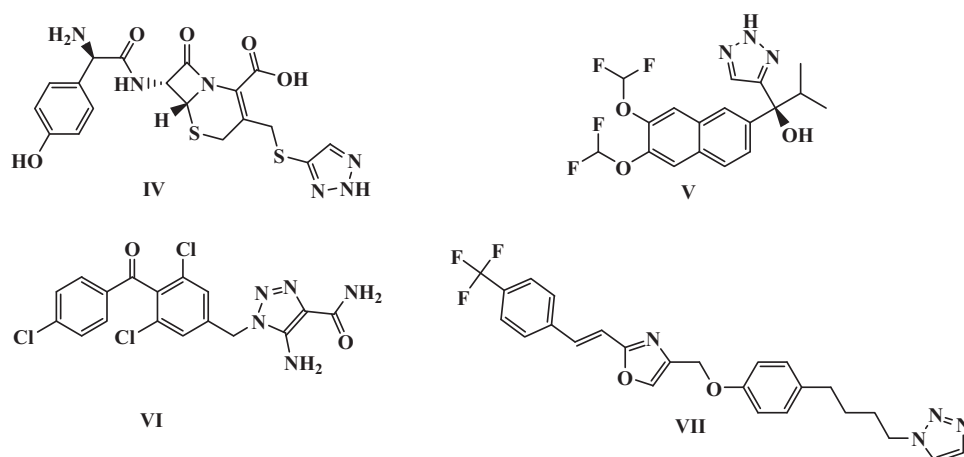


Figure 2. Potential anticancer drugs based on 1,2,3-triazole nucleus in active clinical trials.

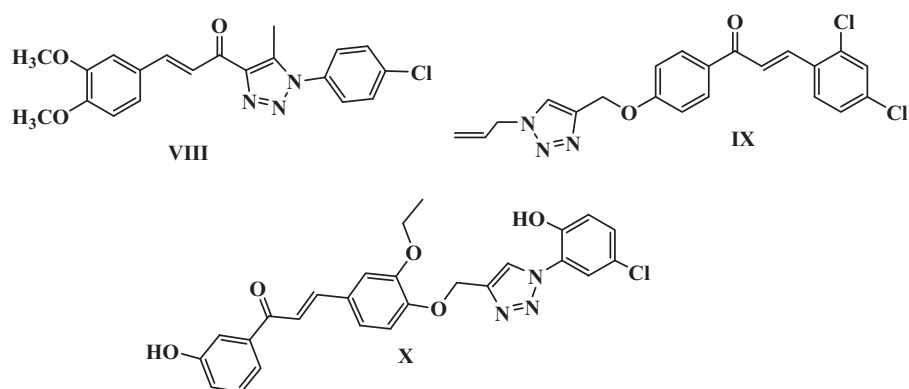


Figure 3. Some recently reported anti-proliferative 1,2,3-triazole/chalcone hybrids.

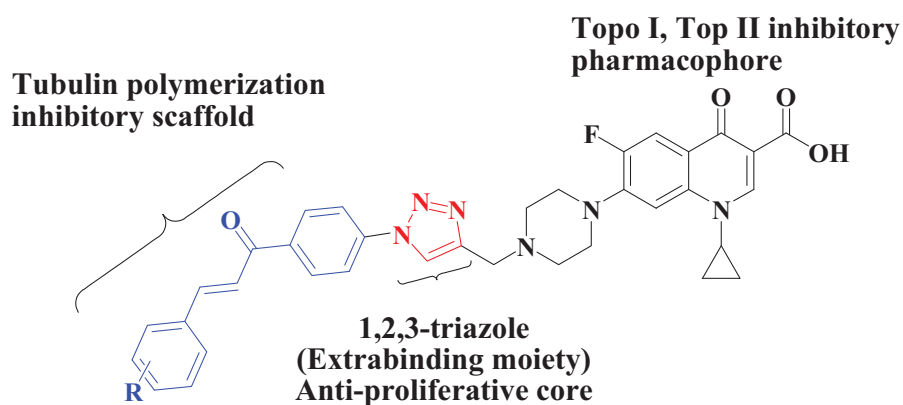
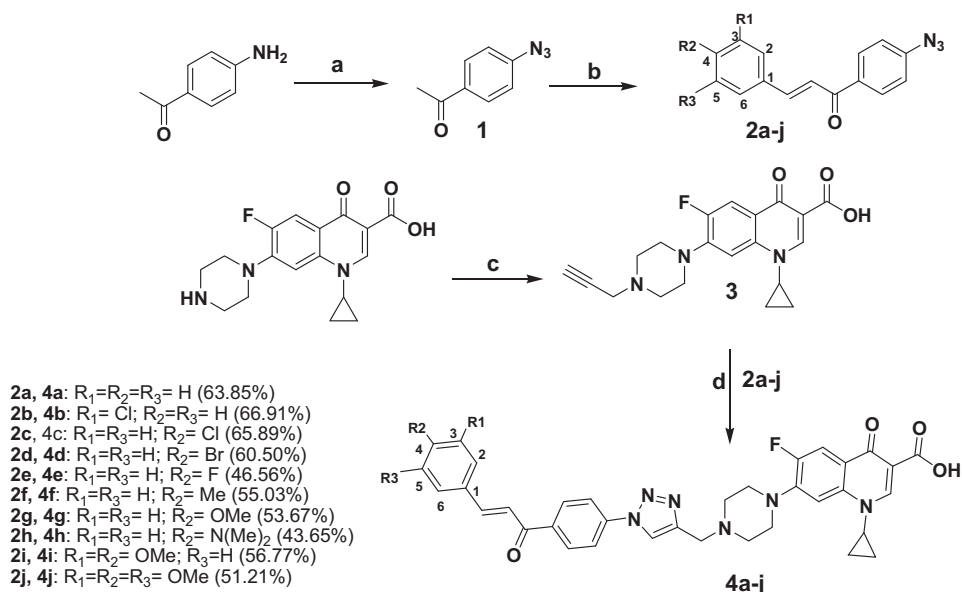


Figure 4. Pharmacophore of target compounds 4a-j.



Scheme 1. Reagents and conditions: (a) Conc. H₂SO₄, NaNO₂, NaN₃, 0–5 °C; (b) Proper aromatic aldehydes, 60% sodium hydroxide, ethanol, stirred overnight at 0–5 °C; (c) Propargyl bromide, NaHCO₃, DMF, stirred overnight at 80 °C; (d) CuSO₄·5H₂O, Sodium ascorbate, DMF, CH₂Cl₂, MeOH, H₂O (3:2:1:1) rt stirring 24 h.

2.2. Biological investigations

2.2.1. Cytotoxic studies

2.2.1.1. *In-vitro* single-dose experiment. For screening of anticancer properties, all the developed compounds were chosen by the

(NCI) for *in-vitro* antitumor evaluation. The assay was carried out using 59 human cancer cell lines obtained from nine tumour sub-panels (breast, ovarian, melanoma, leukaemia, renal, CNS, lung, prostate, and colon cancer cell lines). Compounds were assessed

at a 10 μM concentration. The results of anticancer screening (as shown in Table 1 in Supplementary Data) indicated that all the synthesised CP derivatives produced remarkable anti-proliferative effects against leukaemia (RPMI-8226 and SR) and colon (HCT116) tumour cells with a growth percent ranged from 47.83 to -53.36% . Among the tested compounds, CP hybrid **4j** exhibited a strong and wide range of anti-proliferative activities in the majority of cancer cell lines with a growth percent ranged from 67.46 to -39.69% . Also, hybrids **4a**, **4b**, **4e**, **4i** and **4j** produced significant anti-proliferative effect in several cancer cells, particularly in leukaemia (RPMI-8226) and colon (HCT116) cells with growth percent of 47.87, -14.59 , -24.56 , -24.42 , -15.84 , -9.74 , -53.36 , -10.26 , -31.29 , and -39.51% , respectively.

2.2.1.2 In-vitro five-dose experiment. Showing promising results in the single-dose assay, compound **4j** was advanced for further investigation against a panel of 59 human cancer cell-lines at a five-dose levels. Those cell lines represent nine different tumours, and they were all incubated with our compound at 5 increasing concentrations (0.01, 0.1, 1, 10 and 100 μM). The *In-vitro* five-dose assay results were listed in Table 1, as GI_{50} which is the concentration causes 50% inhibition of cell proliferation and it was expressed in μM . Moreover, Total growth inhibition concentration (TGI) in μM was calculated and listed in Table 1. Results showed that compound **4j** displayed high activity and a wide range of antitumor effects with no selectivity towards all cancer cell lines with GI_{50} values between 0.21 μM and 21.10 μM with selectivity ratio from 0.67 to 1.69 μM at GI_{50} level, as shown in Table 1.

Table 1. GI_{50} in μM and total growth inhibition (TGI) in μM of compound **4j** against 59 cell lines of nine cancer panels evaluated using NCI's *in-vitro* 5-dose antitumor assay.

Panel/Cell line	GI_{50} (μM)	TGI (μM)	Panel/Cell line	GI_{50} (μM)	TGI (μM)
Leukaemia			Melanoma		
CCRF-CEM	2.63	>100	LOX IMVI	1.57	nd
HL-60(TB)	3.18	>100	MALME-3M	2.59	8.41
K-562	0.97	>100	M14	2.49	nd
MOLT-4	3.32	>100	MDA-MB-435	1.49	4.67
RPMI-8226	0.40	4.46	SK-MEL-2	21.10	>100
SR	0.43	>100	SK-MEL-28	2.77	10.40
SK-MEL-5			SK-MEL-5	2.64	7.74
Non-small cell lung cancer			Ovarian Cancer		
A549/ATCC	2.98	>100	UACC-257	6.34	>100
EKVX	4.24	>100	UACC-62	2.83	8.84
HOP-62	2.49	>100		1.73	3.43
HOP-92	11.70	38.30	IGROV1	1.64	4.04
NCI-H226	2.39	6.63	OVCAR-3	1.84	4.93
NCI-H23	2.97	22.30	OVCAR-4	3.94	15.50
NCI-H322M	3.58	>100	OVCAR-5	3.70	25.70
NCI-H460	2.40	6.66	OVCAR-8	4.03	>100
NCI-H522	4.25	>100	NCI/ADR-RES	>100	>100
Colon cancer			SK-OV-3	7.09	>100
COLO 205	5.08	>100	Renal Cancer		
HCC-2998	1.73	4.08	786-0	1.67	3.39
HCT-116	0.21	0.54	A498	4.18	14.40
HCT-15	2.25	>100	ACHN	3.50	45.20
HT29	1.24	>100	CAKI-1	5.10	19.00
KM12	1.57	4.46	SN12C	2.66	10.00
SW-620	1.37	6.98	TK-10	5.61	>100
CNS cancer			UO-31	1.73	9.01
SF-268	3.09	>100	Breast cancer		
SF-295	2.91	>100	MCF7	0.39	>100
SF-539	1.91	4.39	MDA-MB231/ATCC	3.20	>100
SNB-19	4.52	0.67	HS 578 T	3.91	>100
SNB-75	1.49	4.29	BT-549	1.71	3.76
U251	1.48	>100	T-47D	3.16	>100
Prostate cancer			MDA-MB-468	1.96	5.24
PC-3	2.54	15.70			
DU-145	3.67	34.90			

Furthermore, compound **4j** displayed the capacity to achieve total growth inhibition (TGI) against thirty-one cell lines with TGI values between 0.54 and 45.20 μM .

2.2.1.3. In-vitro anti-proliferative study using HCT116, HT29, and Caco-2 cells. As the one dose experiment showed remarkable growth inhibition of the synthesised compounds against the colon cancer cells, we determined the IC_{50} s of the target hybrid compounds **4a-j** against three human colon cancer cell lines (Caco-2, HT-29, and HCT116) using the MTT assay after 24 h incubation period. Results in Table 2 showed that the new CP hybrids **4a-j** had stronger anti-proliferative effects in HCT116 cells (IC_{50} range 2.53–8.67 μM) than H29 cells (IC_{50} range 8.67–62.47 μM) and Caco-2 cells (IC_{50} range 4.19–24.37 μM). Compounds **4a**, **4b**, **4e**, **4i**, and **4j** displayed noticeable anti-proliferative effects against the colon cancer cells. Among the tested compounds, the unsubstituted (**4a**) and 3,4,5-trimethoxy (**4j**) derivatives exhibited the strongest anti-proliferative effect. Also, the results indicated that biological activity is not affected by the electronic effect of the substituents. However, the **4j** showed the highest cytotoxic effect against HCT116 cells, we noticed difference in the IC_{50} values of **4j** between using the SRB assay ($\text{IC}_{50} = 0.2 \mu\text{M}$) and the MTT assay ($\text{IC}_{50} = 2.53 \mu\text{M}$). We assume this difference is due to the SRB assay is more sensitive than the MTT assay as previously described in the literature^{68,69}. Simple structure-activity relationship (SAR) based on HCT-116 cytotoxicity data showed that the absence of substituents on the aromatic ring is favourable to any substituted except 3,4,5-trimethoxy substituents (compound **4j**). For monosubstituted derivatives, the fluorine atom in position 4 is optimal for activity over other donating groups or halogens at the same position. Additionally, the anti-proliferative activity increased with decreasing the halogen size as follows 4-Br < 4-Cl < 4-F.

2.2.1.4. Effect of ciprofloxacin-chalcone hybrids on non-cancerous cells. To evaluate the selectivity and safety profile of the synthesised CP hybrids, a cytotoxicity experiment of compounds **4a**, **4b**, **4e**, **4i**, and **4j** was performed using normal Human Embryonic Kidney (HEK) 293 cells. Results obtained from cytotoxicity assay showed that CP hybrids **4a**, **4b**, **4e**, **4i**, and **4j** caused cytotoxic effects in HEK293 cells to different extents after 72 h incubation period with IC_{50} s ranging from 0.6523 μM to 10.1600 μM , but their cytotoxicity were much lower than that of doxorubicin cytotoxicity in HEK293 which had IC_{50} equal to 0.0475 μM (Figure 5(A)). CP hybrid **4j** had the steepest concentration-cell viability curve of any other ciprofloxacin-chalcone hybrids against HEK293 cells, suggesting that the **4j** compound had stronger cytotoxic activity than other ciprofloxacin-chalcone hybrids. However, the concentration-cell viability curve of **4j** was shallower than the dose-response curve of doxorubicin (positive control). This demonstrates that our

Table 2: Cytotoxic effects of CP hybrids, **4a-j** and doxorubicin against 3 colon cancer cell lines (Caco-2, HT-29, and HCT116).

Compound	HCT116	HT-29	Caco-2
4a	3.57 \pm 0.59	22.35 \pm 3.25	8.39 \pm 2.46
4b	4.81 \pm 1.21	42.91 \pm 5.14	24.37 \pm 3.07
4c	6.45 \pm 1.84	15.34 \pm 1.54	11.73 \pm 2.95
4d	8.67 \pm 2.15	62.47 \pm 7.10	7.19 \pm 1.69
4e	4.32 \pm 0.98	8.67 \pm 2.94	4.19 \pm 1.13
4f	7.22 \pm 1.45	14.71 \pm 1.81	10.05 \pm 2.82
4g	6.11 \pm 1.03	34.01 \pm 3.69	11.41 \pm 3.19
4h	5.09 \pm 2.74	21.74 \pm 2.74	6.39 \pm 1.41
4i	4.87 \pm 0.78	18.60 \pm 3.19	11.28 \pm 2.39
4j	2.53 \pm 0.31	13.24 \pm 2.40	7.14 \pm 2.48
Doxorubicin	1.22 \pm 0.27	0.88 \pm 0.58	4.15 \pm 1.08

synthesised CP hybrids are less cytotoxic against non-cancerous cells (HEK293) when compared to the commonly used chemotherapy (doxorubicin). Further analysis of the cytotoxicity data revealed that CP hybrids (**4a**, **4b**, **4e**, and **4i**) had significantly larger IC_{50} values ($p \leq 0.0001$, Figure 5(B)). Also, the **4j** compound had a higher IC_{50} value than doxorubicin albeit not significantly different. These findings were further supported by microscopic images of cells treated with different concentrations of these compounds (Figure 5(C,D)). The cytotoxic effects of CP hybrids in HEK293 may be due to the long incubation period compared to the incubation period of HCT116 cells. Furthermore, compound **4j**, a more cytotoxic hybrid, had a selectivity index six-fold better than that of the drug Doxorubicin.

2.2.2. Effects of compounds **4a**, **4b**, **4e**, **4i**, and **4j** on topoisomerase I/II inhibitory activity

Based on our design, we hypothesised that the new CP hybrids **4a-j** could act as multi-target ligands that can block the catalytic activity of topoisomerases I (Topo-I), topoisomerases (Topo-II), and inhibit tubulin polymerisation as possible targets for the anti-proliferative

activity. First, the Topo-I activity was tested by the DNA relaxation assay. The supercoiled plasmid has been utilised as a substrate in the relaxation assay to study the inhibition of DNA Topo-I activity. The relaxed isomers migrate in the gel more slowly than the supercoiled isomers; hence they can be distinguished from each other. If the synthesised compounds have an inhibitory effect on the catalytic activity of Topo-I, the DNA molecules will remain in the supercoiled form, a faster moving single band. As shown in (Figure 6(A)), we determined that **4a**, **4b**, **4e**, **4i**, and **4j** could inhibit Topo-I catalytic activity, with **4a** the most potent Topo-I inhibitor.

Moreover, the Topo-I enzymatic activity inhibition by the synthesised compounds was confirmed using the Human DNA Topoisomerase I Assay Kit (ProFoldin, Hudson, MA, USA) (Figure 6(B)). The results of Human DNA Topoisomerase I Assay as shown in (Figure 6(B)) indicated that compound **4a** had the highest Topo-I inhibitory activity which was slightly higher than that of the reference camptothecin. On the other hand, compound **4j** was the less potent Topo-I inhibitor.

The remarkable Topo-I inhibitory activities of the synthesised hybrids; **4a**, **4b**, **4e**, **4i**, and **4j** are in agreement with our hypotheses of these hybrid as Topo-I inhibitors.

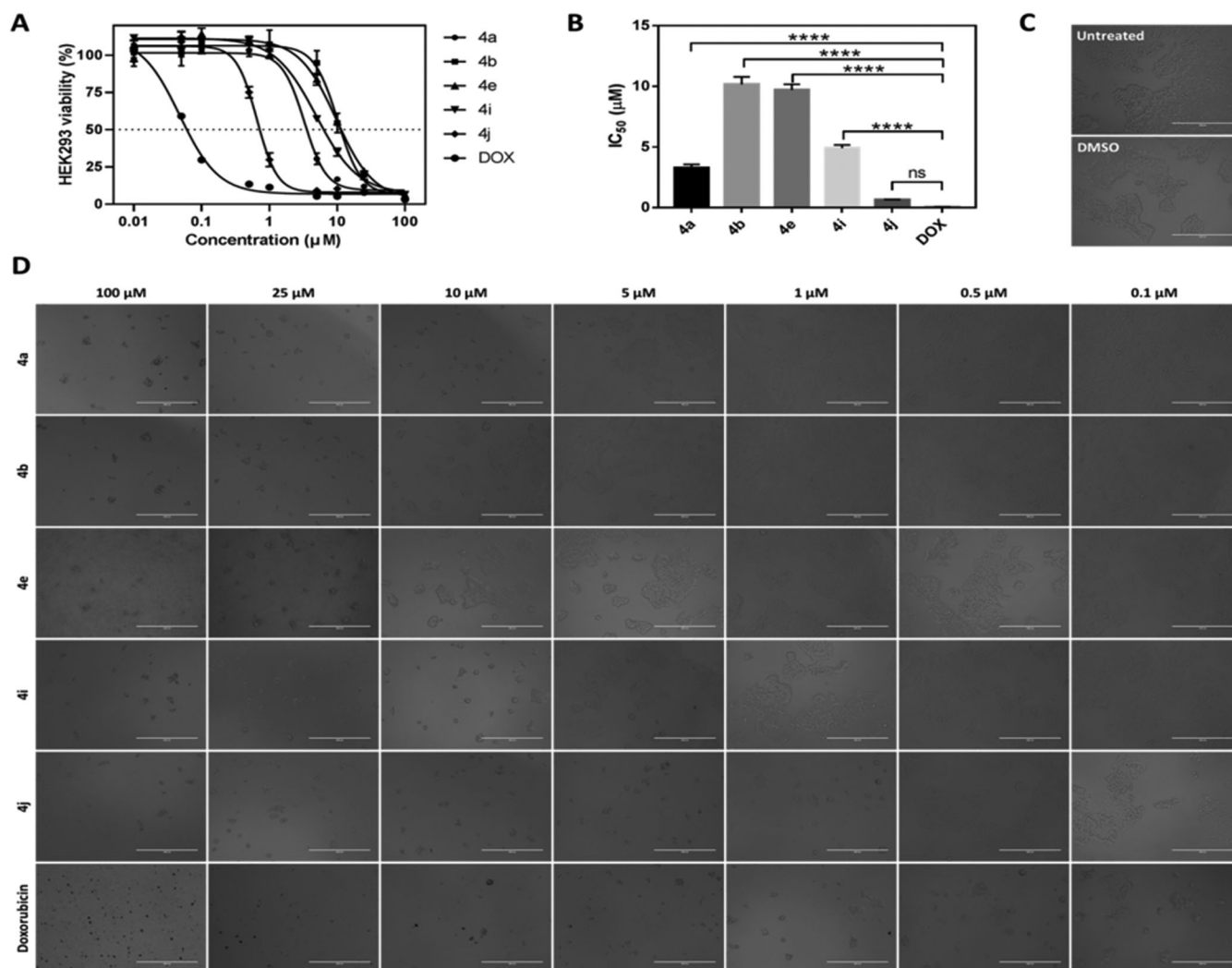


Figure 5. Cytotoxic effects of CP hybrids (**4a**, **4b**, **4e**, **4i**, and **4j**) and doxorubicin against non-cancerous cells (HEK293) after 72 h incubation period. (A) Concentration-cell viability curves of CP hybrids and doxorubicin treated HEK293 cells using different concentrations (0.01–100 μM , $n = 3$) and 72 h incubation period. (B) IC_{50} values were estimated by fitting the cytotoxicity data into a linear regression model using GraphPad Prism software. Data were statistically compared by one-way ANOVA followed by Tukey's multiple comparisons test (**** $p < 0.0001$, ns = not significant). (C and D). Microscopic images of HEK293 cells treated with different concentrations of CP hybrids (**4a**, **4b**, **4e**, **4i**, and **4j**) and doxorubicin for 72 h (20 \times objective lens, total magnification = 200 \times). Scale bar = 400 μM .

Second, the inhibitory activity of Topo II α was evaluated for compounds **4a**, **4b**, **4e**, **4i**, and **4j** utilising Human Topoisomerase II assay kit (TG1001, Topogen Inc.). Etoposide, known inhibitor of Topo II α , was used as reference. Topo-II assay results indicated that the synthesised CP hybrids exhibited strong Topo-II inhibitory activity when compared to the positive control, etoposide (ETO) (Figure 7(A)). Based on the analysis of band intensity using ImageJ software, it was found that all CP hybrids inhibited Topo-II to a similar magnitude in comparison to ETO when 100 μ M of each compound was used (Figure 7(B)). However, when a lower concentration (10 μ M) was tested, it was found that three ciprofloxacin hybrids (**4a**, **4e**, and **4j**) had stronger inhibitory activity than **4b**, **4i**, and ETO. The above results are compatible with our design of these hybrids as Topo-II inhibitors. According to these results, CP hybrid **4a** had the strongest inhibitory activity on both Topo-I and Topo-II enzymes.

2.2.3. Effects of compounds **4a**, **4b**, **4e**, **4i**, and **4j** on tubulin polymerisation

The process of tubulin polymerisation in the cells is important for the completion of mitosis and is targeted for cancer treatment. It has been reported that the suppression of tubulin polymerisation will arrest the cells at the G2/M and it eventually leads to cell death. To test the tubulin-disruptive effect of the CP hybrids, HCT116 cells were analysed by immunocytochemistry. HCT116 cells were incubated for 36 h with IC₅₀ of the CP hybrids (**4a**, **4b**, **4e**, **4i**, and **4j**), nocodazole (a well-known tubulin polymerisation inhibitor, as a positive control), DMSO or Paclitaxel (a well-known tubulin polymerisation inducer, as a negative control), and tubulin was visualised by immunofluorescence microscopy. An antibody for α -tubulin was used. Untreated and Paclitaxel treated HCT116 cells showed a spider-web-like structure (Figure 8). Morphological changes of HCT116 cells treated with either CP hybrids (**4a**, **4b**, **4e**, **4i**, and **4j**) or nocodazole showed a significant tubulin polymerisation inhibition (Figure 8(A)). Moreover, a Western blot was performed to verify the tubulin polymerisation inhibition ability of the synthesised compounds (Figure 8(B)). The level of polymerised tubulin was decreased in HCT116 cells treated with IC₅₀ values of CP hybrids **4a**, **4b**, **4e**, **4i**, **4j**, or nocodazole. Additionally, compounds **4i** and **4j** showed potent inhibition of tubulin polymerisation (Figure 8) and a similar weak effect on human topoisomerase I activity which may suggest that the tubulin inhibition mechanism is the primary mechanism of action for these compounds. The

above-mentioned findings indicated that the synthesised compounds could act as multi-targets; Topo-I, Topo-II, and tubulin polymerisation inhibitors as intended by our design.

2.2.4. DNA damage induction upon treatment with compounds **4a**, **4b**, **4e**, **4i**, and **4j**

DNA damage is a major reason for inhibiting proliferation and inducing cytotoxicity in cancer cells as well as the main downstream cascade for the Topo-I, Topo-II, and tubulin polymerisation inhibition. The phosphorylation of the histone H2AX always occurs after DNA damage forming double-stranded breaks (DSBs). Therefore, we tested the capability of the potent prepared compounds to trigger DNA double strand breaks through detection of the phosphorylation of γ H2AX using two different techniques, Immunofluorescence, and western blotting. Results in (Figure 9(A,B)) indicated that treatment of HCT116 cells with the IC₅₀ of the potent compounds (**4a**, **4b**, **4e**, **4i**, and **4j**) induced γ H2AX foci formation. Also, more γ H2AX-positive cells were observed in comparison to the control cells. Similarly, the western blotting analysis (Figure 9(C,D)) showed increases in the γ H2AX protein expression in cells treated with the IC₅₀ of the target compounds (**4a**, **4b**, **4e**, **4i**, and **4j**) in comparison with the control cells. These results clearly show that the 1,2,3-Triazole linked CP hybrids induce DNA damage in colon cancer cells.

2.2.5. Effects of compounds **4a**, **4b**, **4e**, **4i**, and **4j** on cell cycle analysis

Generally, the mammalian cells counteract the DNA damage by different mechanisms including the cell cycle arrest to allow the cell to repair the damage. There are 2 checkpoints that control DNA damage. The first checkpoint is at the G1/S transition while the other checkpoint is at the G2/M transition. To cover the mechanisms of the synthesised compounds in inhibiting cell proliferation, we analysed the distribution of cell cycle of HCT116 cells following the treatment with different doses of **4a**, **4b**, **4e**, **4i**, and **4j**. The result showed that **4a**, **4b**, **4e**, **4i**, and **4j** induced G2/M phase cell cycle arrest in a concentration-dependent manner (Figure 10). Our results suggest that 1,2,3-Triazole linked CP-Chalcone hybrids arrest the cell cycle of colon tumour cells in G2/M phase.

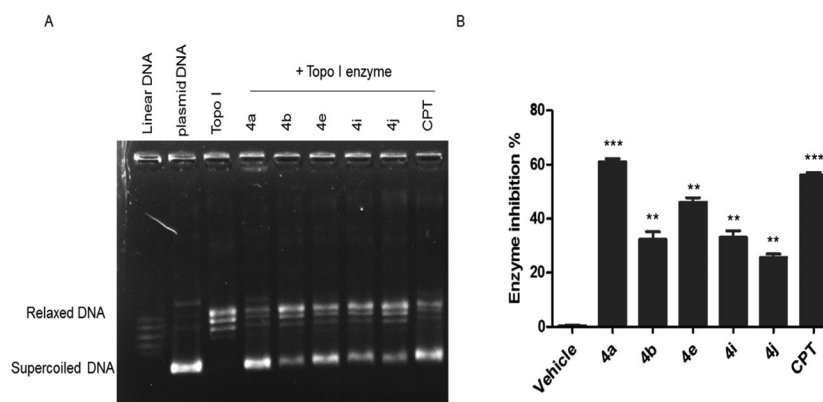


Figure 6. The effect of IC₅₀ values of CP hybrids **4a**, **4b**, **4e**, **4i**, **4j** and camptothecin (CPT, positive control in Topo-I assay) on the activity of human topoisomerase I. (A) DNA relaxation assay. (B) *in-vitro* enzyme assay. Data are plotted as means \pm SEM of 3 experiments. ** $p < 0.01$ and *** $p < 0.001$ refer to the statistically significant differences in comparison to DMSO (vehicle, negative control treatment).

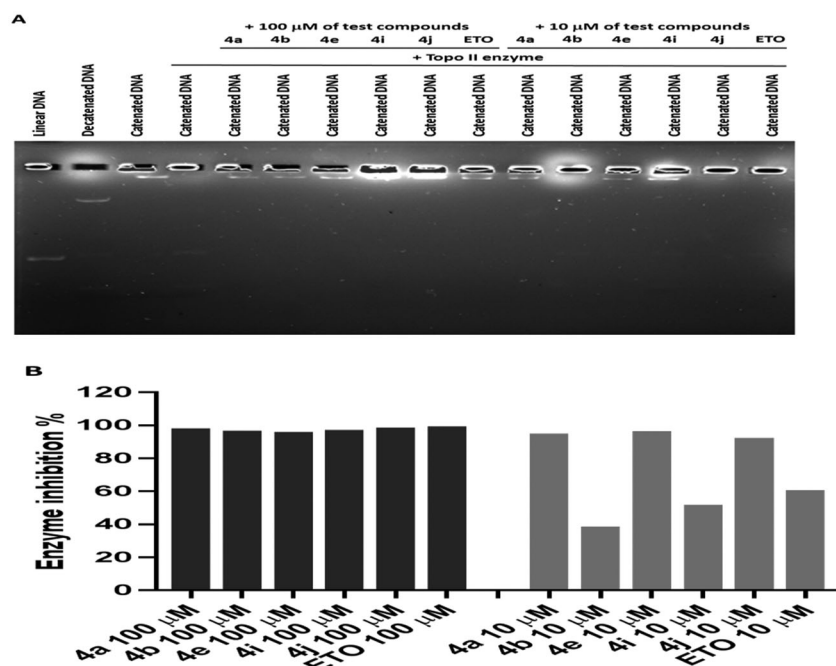


Figure 7. The effect of ciprofloxacin hybrids 4a, 4b, 4e, 4i, 4j, and etoposide (ETO, positive control in Topo-II assay) on the activity of human topoisomerase II. (A). Agarose gel electrophoresis of human topoisomerase II assay. (B). Topo-II inhibitory activity of ciprofloxacin hybrids.

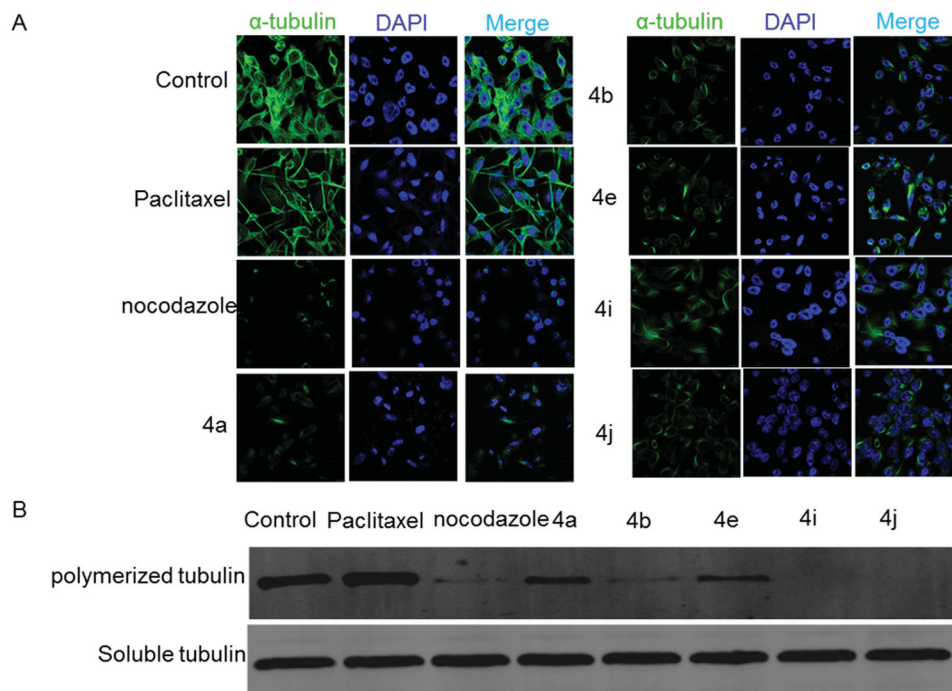


Figure 8. Effect of ciprofloxacin derivatives on tubulin polymerisation. HCT116 cells were untreated (control) and treated with IC_{50} values of compounds 4a, 4b, 4e, 4i, 4j, paclitaxel or nocodazole for 36 h. (A) Morphological changes of HCT116 cells visualised by immunofluorescence microscopy. Tubulin were shown in green and the nuclei were in blue. (B) Western blotting analysis.

2.2.6. Effects of compounds 4a, 4b, 4e, 4i, and 4j on activation of the ATR-Chk1-Cdc25C Cascade

To clarify the molecular mechanism responsible for inducing G₂/M phase arrest in HCT116 following the treatment with the synthesised compounds, the signalling in the checkpoint pathway that regulates the G₂/M transition was investigated. The mammalian cells

respond to the DNA damage through 2 different kinase-signalling cascades (ATR-Chk1 and ATM-Chk2). First, the effect of the synthesised compounds on ATM and ATR phosphorylation was tested. It was found that the ATM phosphorylation on Ser-1981 was unchanged in the comparison with the control (data not shown) after treatment with the synthesised compounds, while p-ATR at

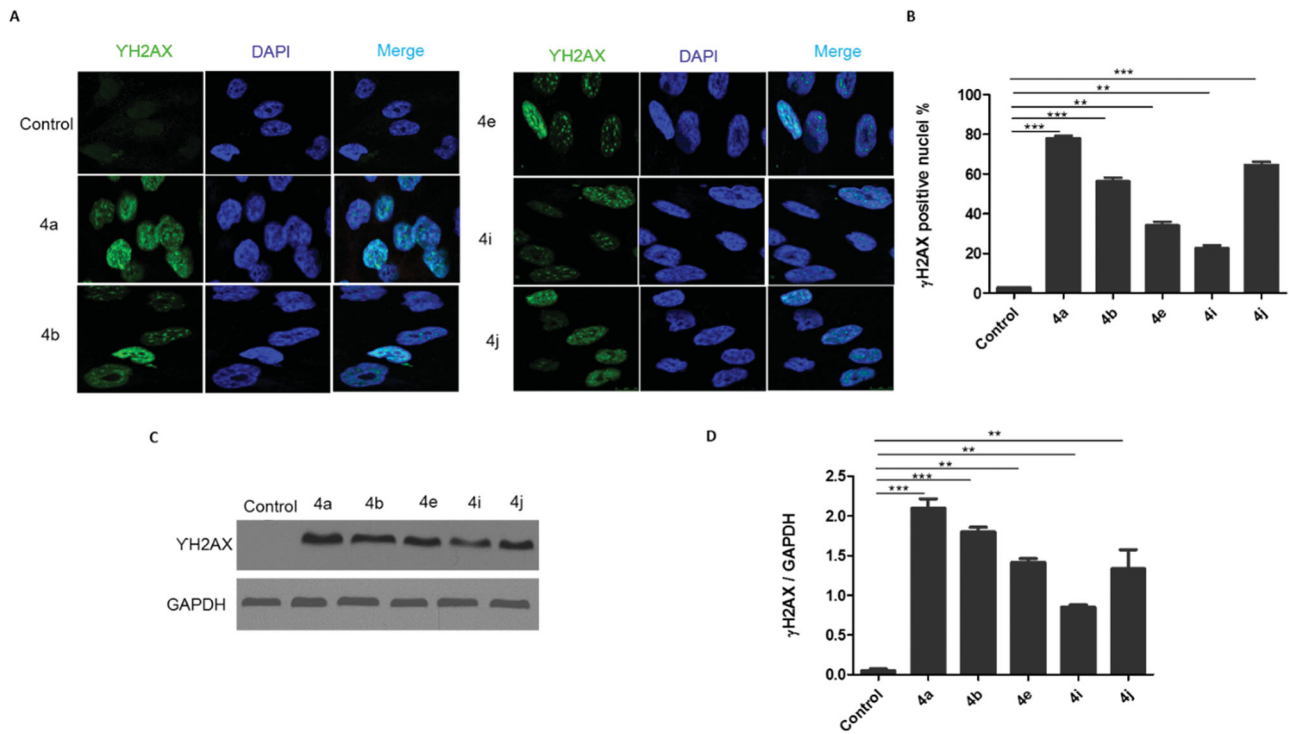


Figure 9. CP hybrids induce DNA damage. (A) γ H2AX staining in HCT116 cells treated with IC_{50} values of CP hybrids 4a, 4b, 4e, 4i, 4j, or DMSO (negative control). (B) γ H2AX-positive nuclei %. (C) Western blot revealed that levels of γ H2AX were increased in HCT116 cells treated with CP hybrids 4a, 4b, 4e, 4i, 4j, DMSO (negative control), and GAPDH (loading control). (D) The relative protein level of γ -H2AX, in comparison to GAPDH was measured by ImageJ. Data are plotted as means \pm SEM of 3 experiments. * $p < 0.05$, ** $p < 0.01$, and *** $p < 0.001$ refer to the statistically significant differences in comparison to DMSO.

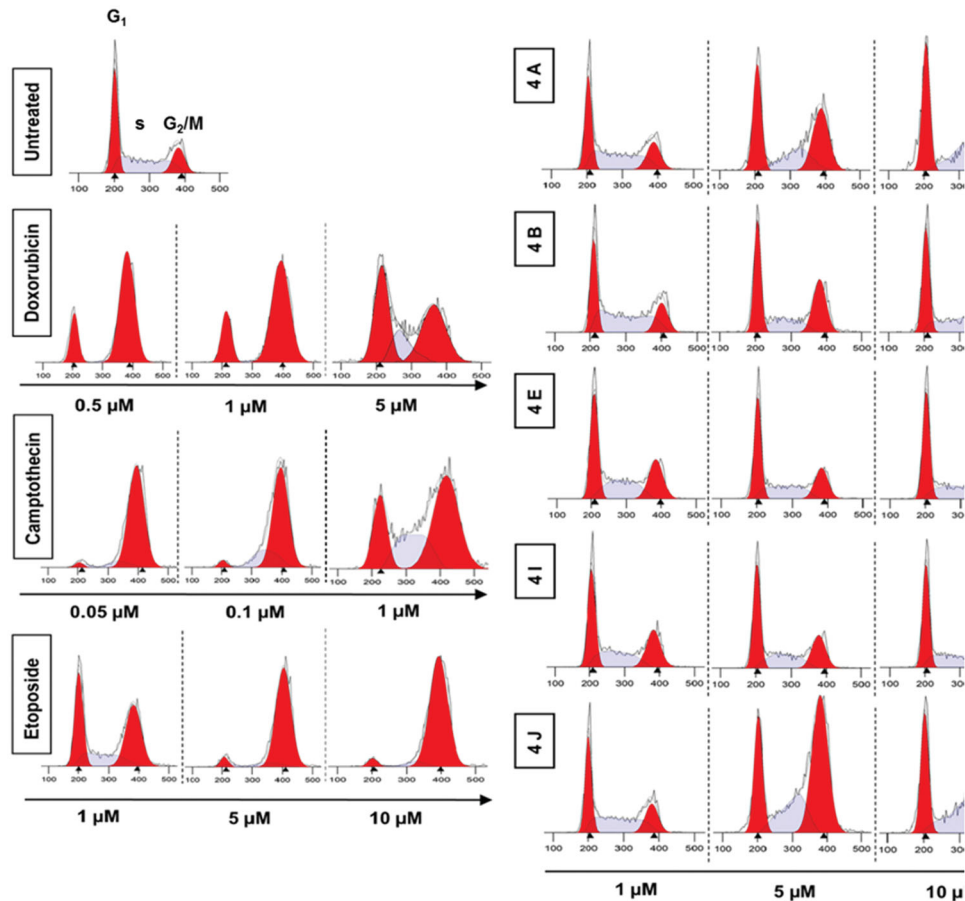


Figure 10. Analysis of cell cycle. HCT116 cells were treated with different concentrations of ciprofloxacin hybrids 4a, 4b, 4e, 4i, and 4j for 24 h. Doxorubicin, camptothecin, and etoposide were used as assay controls. The X-axis displays the fluorescence intensity corresponding to the DNA content per HCT116 cell. DNA histograms were analysed by ModFit LT software.

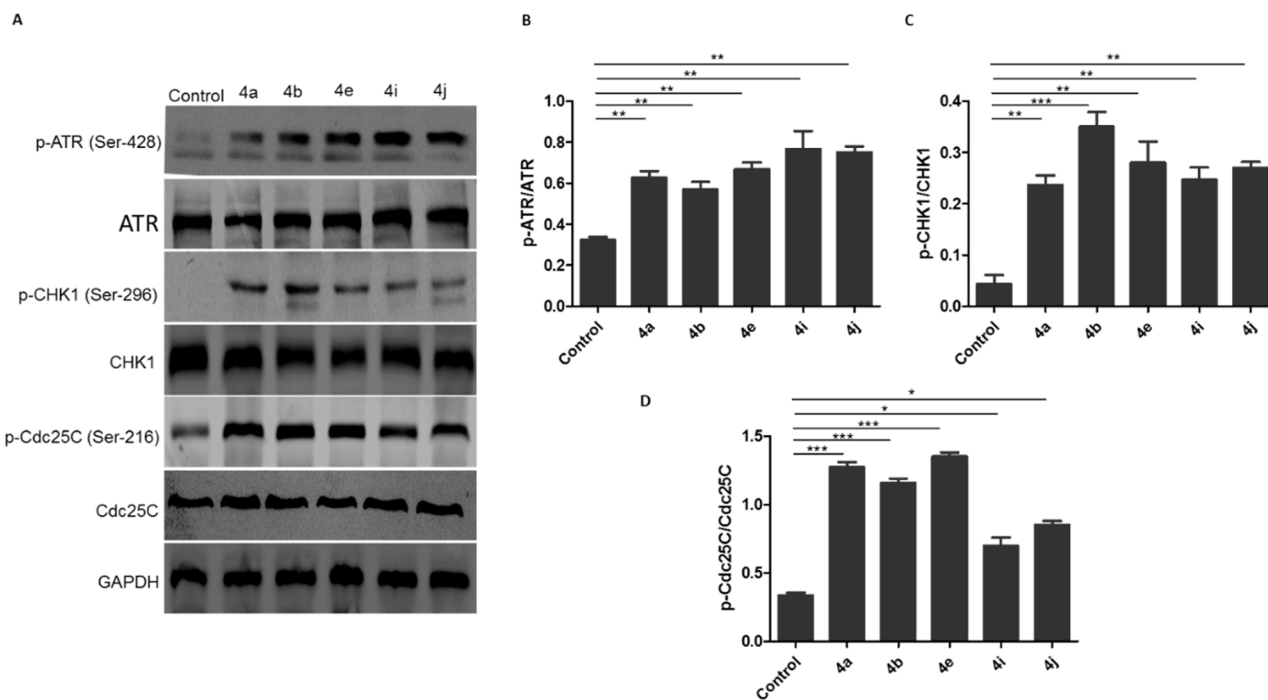


Figure 11. Ciprofloxacin hybrids **4a**, **4b**, **4e**, **4i**, and **4j** induce G₂/M cell cycle arrest possibly via ATR/CHK1/Cdc25C pathway. A. Western blot revealed that expressions of p-ATR, p-CHK1, and p-Cdc25C were increased in HCT116 cells treated with Ciprofloxacin hybrids **4a**, **4b**, **4e**, **4i**, **4j**, DMSO (negative control), and GAPDH (loading control). B. The relative protein levels of p-ATR, p-CHK1, and p-Cdc25C, compared to their total form ATR, CHK1, and Cdc25C, respectively, were measured by ImageJ. Data are plotted as means \pm SEM of 3 experiments. * $p < 0.05$, ** $p < 0.01$, and *** $p < 0.001$ refer to the statistically significant differences in comparison to DMSO.

Table 3. ΔG values of the tested compounds **4a**, **4b**, **4e**, **4i**, **4j**, and camptothecin in the active binding site of Topo I enzyme (PDB ID: **1T8I**).

Compound	ΔG values (kcal/mol)
4a	-10.905
4b	-11.622
4e	-11.154
4i	-11.738
4j	-13.267
Camptothecin	-9.761

Ser-428 markedly increased (Figure 11(A,B)). Then, the phosphorylation of downstream effectors of ATM/ATR, phospho-Chk1-S269, and phospho-Chk2-T68 kinases was explored. It was observed that the synthesised compounds upregulated the phosphorylation of Chk1 at S269 (Figure 11(A,C)) without affecting the phosphorylation of Chk2 at Thr-68 (data not shown). It is well known that *in vitro* activation of Chk1 phosphorylates Cdc25C on serine-216. Therefore, the impact of the synthesised compounds on the Cdc25C phosphorylation at Ser-216 was investigated. Results showed that the levels of Cdc25C phosphorylation at Ser-216 were substantially elevated in triazole-treated HCT116 cells (Figure 11(A,D)). Overall, these results show that the synthesised hybrids induce G₂/M cell cycle arrest possibly via ATR/CHK1/Cdc25C pathway.

2.3. Molecular docking studies of ciprofloxacin hybrids **4a**, **4b**, **4e**, **4i**, and **4j** on Top-I and Top-II active sites

2.3.1. Docking Studies of ciprofloxacin hybrids **4a**, **4b**, **4e**, **4i**, and **4j** in human Topo I enzyme (PDB ID: **1T8I**)

Based on the potent inhibitory Top-I activities of the synthesised hybrids, we study *in silico* molecular docking simulations using MOE software for the most active compounds **4a**, **4b**, **4e**, **4i**, and

4j into human Top-I enzyme (PDB ID: **1T8I**) in comparison to camptothecin to examine their binding modes. The validation of the docking method was made by re-docking of the co-crystallized ligand and calculation of RMSD. The RMSD was 0.4626 which means the validity of the docking method. All the tested hybrids had a strong binding affinity to the enzyme as the binding free energy (ΔG) values ranged from -10.905 to -13.267 Kcal/mole which were higher than that of camptothecin ($\Delta G = -9.761$ Kcal/mole), (Table 3).

The Docking results (as shown in Table 2 and Figures 1–3, in Supplementary Data) are in agreement with Top-1 inhibitory activity results and indicate that compounds **4a**, **4e**, and **4i** have comparable binding interactions with Top-I enzyme (PDB ID: **1T8I**) to that of camptothecin which forms 3 H-bond interactions with Asp533, Lys532, and Arg364 and four $\pi \dots \pi$ interactions with DA 113, DC 112, and TGP 111, (Figure 12). On the contrast, compounds **4b** and **4j** have fewer binding interactions with Top-I enzyme (PDB ID: **1T8I**) than that of camptothecin. Concerning compound **4a** which had the most potent Top-I inhibitory activity even higher than that of camptothecin, its docking pose shows one H-bonding interaction with Trp 416, one cation... π interaction with Lys 425 and three $\pi \dots \pi$ interactions with DT 10, TGP 111, and DA 113, as shown in (Figure 12). Additionally, compound **4e**, which had Topo-I inhibitory activity comparable to camptothecin, has two H-bonding interactions with Arg 488 & His 632 and three $\pi \dots$ cation interactions with Trp416, DT 10, and DG 12. On the other side, compound **4j** which was the less potent Top-1 inhibitor among the tested hybrids, it has only one cation... π interaction with Glu 356 and one $\pi \dots \pi$ interaction with DC112. See Supplementary Data. The above docking results indicated that although some of the new hybrids have comparable binding interactions as camptothecin, none of these new compounds have H-bond interactions with the same amino acid residues or

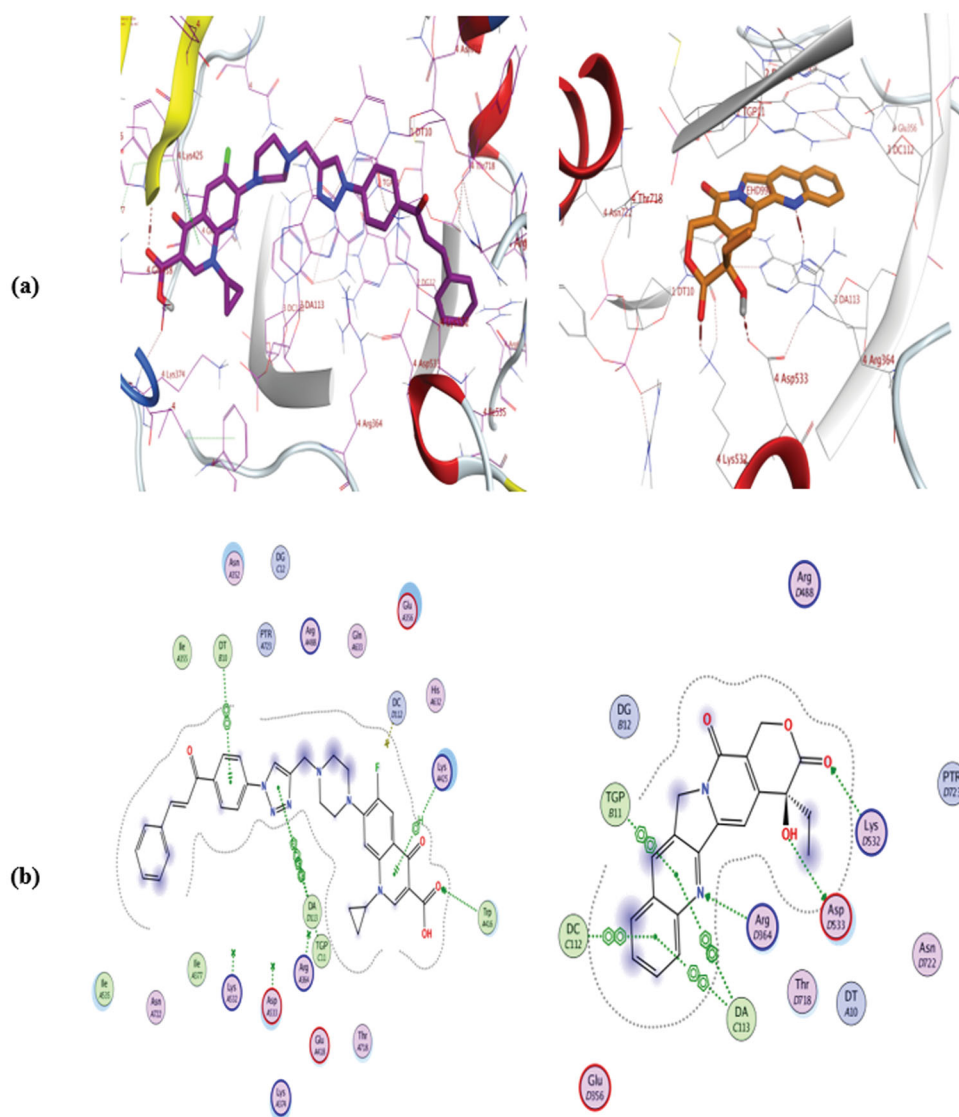


Figure 12. Binding mode and H-bonds interactions of compound **4a** (left) and camptothecin (right) within **1T8I** active site: (a) 3D structure and (b) 2D interactions.

Table 4. ΔG values of the tested compounds **4a**, **4b**, **4e**, **4i**, **4j**, and Etoposide in the active binding site of Topo II enzyme (PDB ID: **6ZY7**).

Compound	ΔG values (kcal/mol)
4a	-9.846
4b	-9.738
4e	-9.511
4i	-9.690
4j	-9.906
Etoposide	-10.162

have three H-bonds like camptothecin, Additionally, none of them have the same number of $\pi \dots \pi$ interactions with the same DNA residues of Top-I enzyme such as camptothecin even the hybrid **4a** which was more potent as Top-1 inhibitor than camptothecin which means these hybrids could have a slight distinct interactions with Top-I enzyme.

2.3.2. Docking studies of ciprofloxacin hybrids **4a**, **4b**, **4e**, **4i**, and **4j** in human Topo II enzyme (PDB ID: **6ZY7**)

Upon relying on the results of the Top II assay, docking of the most active hybrids; **4a**, **4b**, **4e**, **4i**, and **4j**, and the positive

control Etoposide; was performed with the active binding site of into human Topo II enzyme (PDB ID: **6ZY7**) to elucidate their effective binding modes and concentrate on their similarity to the standard ligand binding modes. The docking method validation was examined by re-docking of the co-crystallized Etoposide and calculation of RMSD. The RMSD was 0.4063 which means the docking method is valid. All the tested hybrids had a strong binding affinity to the enzyme as the binding free energy (ΔG) values ranged from -9.511 to -9.906 Kcal/mole which were lower than that of Etoposide ($\Delta G = -10.162$ Kcal/mole), (Table 4).

From the docking, results (as shown in Table 3 and Figures 4–6, in Supplementary Data), we can say that the tested hybrids form different interactions than that of Etoposide which forms four interaction; two hydrogen bonds with DG 13 & DG 5 residues, one $\pi \dots \pi$ cation interaction with DG13, and one $\pi \dots \pi$ interaction with DT 12, (Figure 13). Despite of compounds **4a**, **4e**, and **4j** were more potent as Top-II inhibitors than etoposide at $10 \mu\text{M}$ concentrations. They interact with the **6ZY7** binding site in a different manner with different amino acid residues than that of etoposide. For example, compound **4a** forms only two hydrogen bonds with Ala 465 and Ser 464, (Figure 13). Additionally,

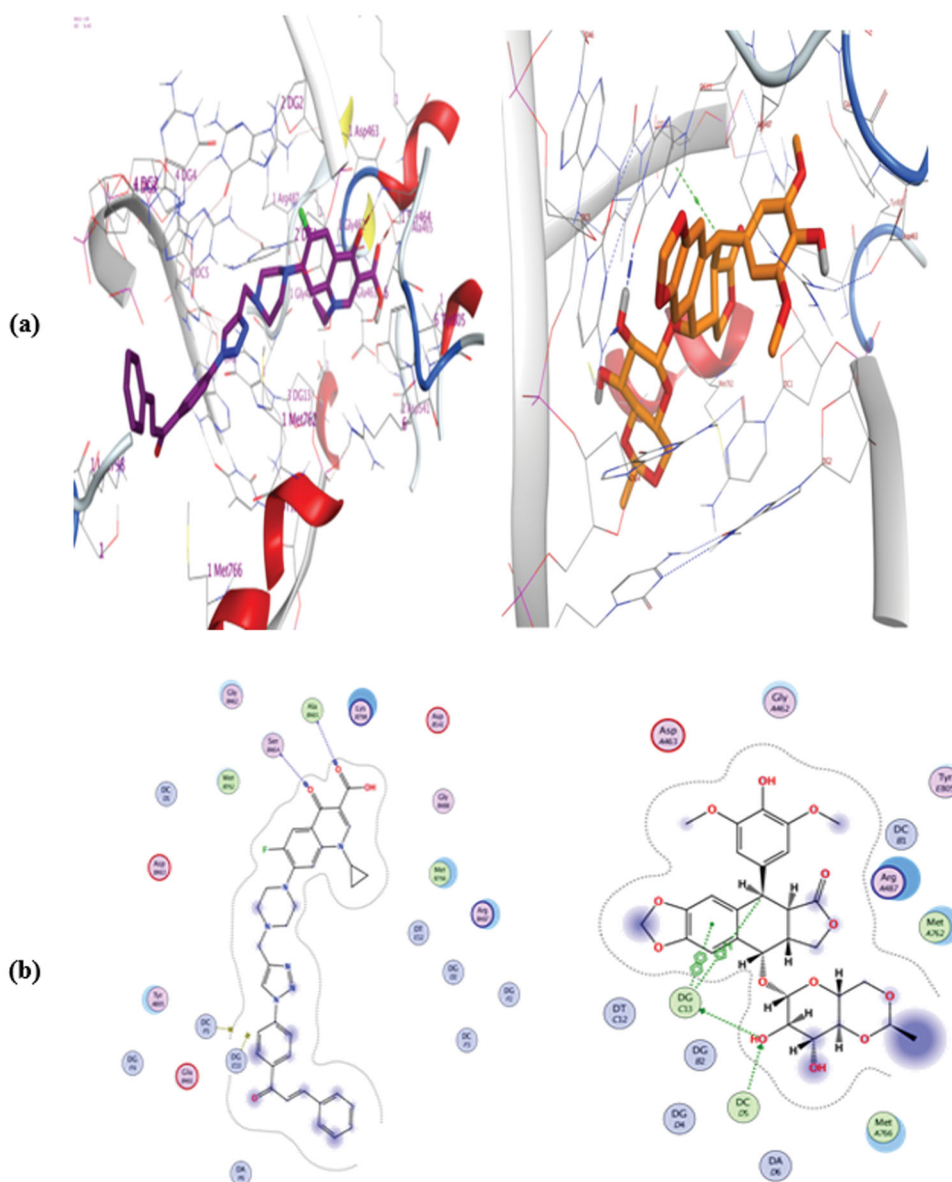


Figure 13. Binding mode and H-bonds interactions of compound **4a** (left) and etoposide (right) within **6ZY7** active site: (a) 3D structure and (b) 2D interactions.

compound **4e** docking pose shows two hydrogen bonds with Ala 801 & Ser 802 and two π ... cation interactions with DT 12 and DG 13. Moreover, **4j** forms only three interactions with the **6ZY7** binding site; two hydrogen bonds with Ser 800 and DC 3 residue and one π ... cation interaction with DC 1 residue. On the other hand, compound **4b** which was less potent Top-II inhibitor among the tested compound at $10\ \mu\text{M}$ forms only one hydrogen bond with Lys- 489.

3. Conclusions

We were successfully able to synthesise novel triazole-linked CP chalcone hybrids **4a-j** with remarkable anti-proliferative activity against leukaemia (RPMI-8226 and SR) and colon (HCT116) tumour cells with a growth percent ranged from 47.87 to -53.36% . Among the tested compounds, CP hybrid **4j** displayed potent and wide-range anti-proliferative effects in the majority of cancer lines with a growth percent range of 67.46 to -39.69% . Also, hybrids **4a**, **4b**, **4e**, **4i**, and **4j** induced significant anti-proliferative effect

in several cancer cells, particularly in leukaemia (RPMI-8226) and colon (HCT116) cell lines with a growth percent values 47.87, -14.59 , -24.56 , -24.42 , -15.84 , -9.74 , -53.36 , -10.26 , -31.29 , and -39.51% , respectively. Generally, the anti-proliferative activity of hybrids **4a-j** was more potent against colon cancer (HCT116) than leukaemia SR (RPMI-8226 and SR) cell lines. Compounds **4a**, **4b**, **4e**, **4i**, and **4j** displayed the strongest anti-proliferative effect in HCT116 cells with $\text{IC}_{50} = 3.57$, 4.81, 4.32, 4.87 and $2.53\ \mu\text{M}$; respectively compared to doxorubicin ($\text{IC}_{50} = 1.22\ \mu\text{M}$). Additionally, Compounds **4a**, **4b**, **4e**, **4i**, and **4j** exhibited much lower toxicity than that of doxorubicin against normal Human Embryonic Kidney (HEK) 293 cells after 72 h incubation period. Also, hybrids **4a**, **4b**, **4e**, **4i**, and **4j** exhibited remarkable inhibitory activities against Topo-I, Topo-II, and tubulin polymerisation compared with the used references. They increased the protein expression level of γH2AX indicating DNA damage (double strand breaks). Furthermore, they arrested the HCT116 cell cycle at the G2/M phase possibly through ATR/CHK1/Cdc25C pathways as a result of DNA damage. Thus, the new CP hybrids have the capacity to be used as promising leads and advanced for further

investigation as novel multi-target anticancer agents to combat colorectal carcinoma.

4. Experimental section

4.1. Chemistry

Thin-layer chromatography (Merck Grade-9385 precoated aluminium TLC plate silica gel 60, size 5 × 20 cm with 0.2 mm thickness) was used to monitor the chemical reaction. Plates were exposed to UV light at a wavelength of 254 nm to detect the spots. In addition, Stuart Electrothermal Melting Point Apparatus was used to determine the melting points (values were un-corrected). Also, 100 MHz for ¹³C and 400 MHz for ¹H NMR spectra were obtained on Bruker AM400 spectrometer using DMSO-*d*₆ (solvent) and tetramethylsilane (internal standard). In this work, δ (chemical shifts) and *J* (coupling constants) were reported in ppm and Hz, respectively. The following abbreviations were used to describe the NMR peak multiplicity: singlet = *s*, doublet = *d*, doublet of doublets = *dd*, triplet = *t*, quartet = *q*, multiplet = *m*, broad signal, *brs*. Shimadzu's GC/MS-QP5050A (Regional Centre for Mycology and Biotechnology, Al-Azhar University, Cairo, Egypt) was used for elemental analyses while Advion's compact mass spectrometer (Nawah Scientific Centre for Research, Almokattam, Cairo, Egypt) was used to obtain mass spectra (*m/z*).

4.1.1. Synthesis of the intermediates; 1, 2a-j, and 3

The intermediate ¹^{65,66}, **2a-j**^{65,66,70}, **3**⁶⁷ were prepared according to the reported methods in the previous studies.

4.1.2. Synthesis of compounds 4a-j

Our target compounds **4a-j** were synthesised by the reaction between Ciprofloxacin alkyne derivative **3** (0.5 g, 1.35 mmol.) and the appropriate azide **2a-j** (0.37 g, 1.48 mmol.) under the catalysis of sodium ascorbate (0.4 eq) and copper (II) sulphate pentahydrate (0.2 eq) as reported procedure⁷¹. See [Supplementary Appendix A](#)

4.1.2.1. (E)-7-(4-((1-(4-(3-(3-chlorophenyl)acryloyl)phenyl)-1H-1,2,3-triazol-4-yl)methyl)piperazin-1-yl)-1-cyclopropyl-6-fluoro-4-oxo-1,4-dihydroquinoline-3-carboxylic acid 4a. Yellowish white powder; (0.53 g, 63.85% yield); mp: 240–242 °C; IR (KBr) ν_{\max} = broad band 3223–3074 cm⁻¹ (OH of COOH), 1715 cm⁻¹ (C=O of COOH), 1657 cm⁻¹ (C=O of CH=CH-C=O) and 1622 (C=O of 4-keto gp of CP); ¹H NMR (400 MHz, DMSO-*d*₆) δ ppm: 1.16–1.22 (2H, m, cyclopropyl-*H*), 1.28–1.36 (2H, m, cyclopropyl-*H*), 2.70–2.80 (4H, m, piperazinyl-*H*), 3.36–3.40 (4H, m, piperazinyl-*H*), 3.77–3.85 (3H, m, *N*-CH₂ and cyclopropyl-1*H*), 7.45–7.60 (4H, m, C8-*H* and Ar-*H*), 7.79 (1H, d, *J*_{trans} = 16 Hz, =CH), 7.83 (1H, d, *J*_{HFortho} = 16 Hz, C5-*H*), 7.90–7.92 (2H, m, Ar-*H*), 7.99 (1H, d, *J*_{trans} = 16 Hz, =CH), 8.15 (2H, d, *J* = 8 Hz, Ar-*H*), 8.35 (2H, d, *J* = 8 Hz, Ar-*H*), 8.62 (1H, s, C2-*H*), 8.93 (1H, s, triazole *H*), 15.14 (1H, brs, COOH); ¹³C NMR (100 MHz, CDCl₃) δ ppm: 8.21, 35.26, 49.51, 51.42, 52.48, 52.90, 104.91, 108.23, 112.48 (C-5, d, ²*J*_{CFortho} = 23 Hz, C-F), 120.12, 121.43, 126.64, 128.57, 129.06, 130.29, 130.91, 134.64, 138.18, 139.08, 140.92, 145.58, 145.81, 146.38, 147.42, 148.43, 153.66 (C-6, d, ¹*J*_{CFipso} = 250 Hz, C-F), 166.89, 177.09, 188.84; ESI-MS (*m/z*): Calcd. 618.24, found 641.60 [M + Na]⁺. Anal. Calcd. For C₃₅H₃₁FN₆O₄: C,

67.95%; H, 5.05%; N, 13.58%. Found: C, 67.84%; H, 5.21%; N, 13.74%.

4.1.2.2. (E)-7-(4-((1-(4-(3-(3-chlorophenyl)acryloyl)phenyl)-1H-1,2,3-triazol-4-yl)methyl)piperazin-1-yl)-1-cyclopropyl-6-fluoro-4-oxo-1,4-dihydroquinoline-3-carboxylic acid 4b. Yellow powder; (0.59 g, 66.91% yield); mp: 254–247 °C; ¹H NMR (400 MHz, DMSO-*d*₆) δ ppm: 1.18–1.24 (2H, m, cyclopropyl-*H*), 1.31–1.35 (2H, m, cyclopropyl-*H*), 2.67–2.73 (4H, m, piperazinyl-*H*), 3.35–3.39 (4H, m, piperazinyl-*H*), 3.79–3.85 (3H, m, *N*-CH₂ and cyclopropyl-1*H*), 7.53–7.60 (2H, m, Ar-*H* and C8-*H*), 7.77 (1H, d, *J*_{trans} = 16 Hz, =CH), 7.84–7.91 (2H, m, Ar-*H* and C5-*H*), 8.09–8.18 (3H, m, =CH and Ar-*H*), 8.17 (2H, d, *J* = 8 Hz, Ar-*H*), 8.42 (2H, d, *J* = 8 Hz, Ar-*H*), 8.65 (1H, s, C2-*H*), 8.92 (1H, s, triazole *H*), 15.17 (1H, brs, COOH); ¹³C NMR (100 MHz, CDCl₃) δ ppm: 7.22, 34.31, 48.34, 50.44, 51.43, 51.85, 103.99, 107.17, 111.43 (C-5, d, ²*J*_{CFortho} = 23 Hz, C-F), 119.17, 121.59, 125.94, 127.03, 129.33, 129.70, 134.14, 135.49, 136.87, 138.08, 138.91, 139.33, 139.84, 142.98, 144.58, 144.76, 146.43, 147.55, 152.64 (C-6, d, ¹*J*_{CFipso} = 250 Hz, C-F), 165.88, 176.05, 187.40; ESI-MS (*m/z*): Calcd. 652.20, found 675.80 [M + Na]⁺. Anal. Calcd. For C₃₅H₃₀ClFN₆O₄: C, 64.37%; H, 4.63%; N, 12.87%. Found: C, 64.53%; H, 4.80%; N, 13.09%.

4.1.2.3. (E)-7-(4-((1-(4-(3-(4-chlorophenyl)acryloyl)phenyl)-1H-1,2,3-triazol-4-yl)methyl)piperazin-1-yl)-1-cyclopropyl-6-fluoro-4-oxo-1,4-dihydroquinoline-3-carboxylic acid 4c. Yellow powder; (0.58 g, 65.89% yield); mp: 257–259 °C; ¹H NMR (400 MHz, DMSO-*d*₆) δ ppm: 1.17–1.22 (2H, m, cyclopropyl-*H*), 1.30–1.35 (2H, m, cyclopropyl-*H*), 2.70–2.76 (4H, m, piperazinyl-*H*), 3.36–3.40 (4H, m, piperazinyl-*H*), 3.80–3.82 (3H, m, *N*-CH₂ and cyclopropyl-1*H*), 7.55 (2H, d, *J* = 8 Hz, Ar-*H*), 7.57 (1H, d, *J*_{Hmeta} = 8 Hz, C8-*H*), 7.79 (1H, d, *J*_{trans} = 16 Hz, =CH), 7.90 (1H, d, *J*_{HFortho} = 12 Hz, C5-*H*), 7.97 (2H, d, *J* = 8 Hz, Ar-*H*), 8.03 (1H, d, *J*_{trans} = 16 Hz, =CH), 8.16 (2H, d, *J* = 8 Hz, Ar-*H*), 8.39 (2H, d, *J* = 8 Hz, Ar-*H*), 8.66 (1H, s, C2-*H*), 8.94 (1H, s, triazole *H*), 15.17 (1H, brs, COOH); ¹³C NMR (100 MHz, CDCl₃) δ ppm: 8.20, 35.28, 49.44, 52.45, 52.88, 104.92, 108.18, 112.42 (C-5, d, ²*J*_{CFortho} = 24 Hz, C-F), 120.12, 121.18, 121.79, 126.33, 129.36, 129.70, 130.27, 133.12, 136.88, 137.97, 139.06, 139.85, 144.22, 144.51, 145.59, 147.40, 153.62 (C-6, d, ¹*J*_{CFipso} = 252 Hz, C-F), 166.85, 177.04, 188.50; ESI-MS (*m/z*): Calcd. 652.20, found 675.80 [M + Na]⁺. Anal. Calcd. For C₃₅H₃₀ClFN₆O₄: C, 64.37%; H, 4.63%; N, 12.87%. Found: C, 64.51%; H, 4.89%; N, 13.04%.

4.1.2.4. (E)-7-(4-((1-(4-(3-(4-bromophenyl)acryloyl)phenyl)-1H-1,2,3-triazol-4-yl)methyl)piperazin-1-yl)-1-cyclopropyl-6-fluoro-4-oxo-1,4-dihydroquinoline-3-carboxylic acid 4d. Pale yellow powder; (0.57 g, 60.50% yield); mp: 247–249 °C; ¹H NMR (400 MHz, DMSO-*d*₆) δ ppm: 1.17–1.21 (2H, m, cyclopropyl-*H*), 1.31–1.35 (2H, m, cyclopropyl-*H*), 2.69–2.75 (4H, m, piperazinyl-*H*), 3.38–3.43 (4H, m, piperazinyl-*H*), 3.81–3.83 (3H, m, *N*-CH₂ and cyclopropyl-1*H*), 7.57 (1H, d, *J*_{Hmeta} = 8 Hz, C8-*H*), 7.68 (2H, d, *J* = 8 Hz, Ar-*H*), 7.76 (1H, d, *J*_{trans} = 16 Hz, =CH), 7.88 (2H, d, *J* = 8 Hz, Ar-*H*), 7.91 (1H, d, *J*_{HFortho} = 12 Hz, C5-*H*), 8.02 (1H, d, *J*_{trans} = 16 Hz, =CH), 8.15 (2H, d, *J* = 8 Hz, Ar-*H*), 8.38 (2H, d, *J* = 8 Hz, Ar-*H*), 8.66 (1H, s, C2-*H*), 8.91 (1H, s, triazole *H*), 15.05 (1H, brs, COOH); ¹³C NMR (100 MHz, CDCl₃) δ ppm: 8.22, 35.30, 49.62, 51.41, 52.22, 104.86, 105.18, 108.18, 112.42 (C-5, d, ²*J*_{CFortho} = 23 Hz, C-F), 120.22, 121.89, 125.24, 129.90, 130.70, 131.08, 131.54, 132.33, 133.55, 138.06, 139.05, 139.74, 144.31, 145.15, 145.81, 153.61 (C-6, d, ¹*J*_{CFipso} = 260 Hz, C-F), 166.90, 177.02,

188.50; ESI-MS (m/z): Calcd. 696.15, found 719.50 $[M + Na]^+$. Anal. Calcd. For $C_{35}H_{30}BrFN_6O_4$: C, 60.26%; H, 4.34%; N, 12.05%. Found: C, 60.53%; H, 4.52%; N, 12.31%.

4.1.2.5. (E)-1-cyclopropyl-6-fluoro-7-(4-((1-(4-(3-(4-fluorophenyl)acryloyl)phenyl)-1H-1,2,3-triazol-4-yl)methyl)piperazin-1-yl)-4-oxo-1,4-dihydroquinoline-3-carboxylic acid 4e. Yellow powder; (0.40 g, 46.56% yield); mp: 203–205 °C; IR (KBr) ν_{max} = broad band 3283–3066 cm^{-1} (OH of COOH), 1718 cm^{-1} (C=O of COOH), 1658 cm^{-1} (C=O of CH=CH-C=O) and 1624 (C=O of 4-keto gp of CP); 1H NMR (400 MHz, DMSO- d_6) δ ppm: 1.17–1.21 (2H, m, cyclopropyl-*H*), 1.31–1.34 (2H, m, cyclopropyl-*H*), 2.75–2.80 (4H, m, piperazinyl-*H*), 3.39–3.45 (4H, m, piperazinyl-*H*), 3.82–3.87 (3H, m, $N-CH_2$ and cyclopropyl-1*H*), 7.30 (2H, t, $J_{HF} = 8$ Hz, Ar-*H*), 7.57 (1H, d, $J_{HFmeta} = 8$ Hz, C8-*H*), 7.79 (1H, d, $J_{trans} = 16$ Hz, =CH), 7.86–7.93 (2H, m, =CH and C5-*H*), 7.97 (2H, d, $J = 8$ Hz, Ar-*H*), 8.13 (2H, d, $J = 8$ Hz, Ar-*H*), 8.35 (2H, d, $J = 8$ Hz, Ar-*H*), 8.66 (1H, s, C2-*H*), 8.86 (1H, s, triazole *H*), 15.05 (1H, brs, COOH); ^{13}C NMR (100 MHz, $CDCl_3$) δ ppm: 6.41, 33.50, 47.43, 50.58, 50.98, 103.22, 106.42, 110.64 (C-5, d, $^2J_{Cortho} = 23$ Hz, C-F), 113.67, 114.46 (C_{Ar}, d, $^2J_{Cortho} = 23$ Hz, C-F), 118.35, 119.38, 119.74, 128.43, 128.67, 128.75, 129.14, 136.36, 137.27, 137.97, 142.62, 143.64, 145.62, 151.82 (C-6, d, $^1J_{CFipso} = 251$ Hz, C-F), 162.53 (C_{Ar}, d, $^1J_{CFipso} = 252$ Hz, C-F), 165.01, 175.23, 186.77; ESI-MS (m/z): Calcd. 636.23, found 659.03 $[M + Na]^+$. Anal. Calcd. For $C_{35}H_{30}F_2N_6O_4$: C, 66.03%; H, 4.75%; N, 13.20%. Found: C, 65.94%; H, 4.89%; N, 12.98%.

4.1.2.6. (E)-1-cyclopropyl-6-fluoro-4-oxo-7-(4-((1-(4-(3-(*p*-tolyl)acryloyl)phenyl)-1H-1,2,3-triazol-4-yl)methyl)piperazin-1-yl)-1,4-dihydroquinoline-3-carboxylic acid 4f. Yellow white powder; (0.47 g, 55.03% yield); mp: 259–261 °C; 1H NMR (400 MHz, DMSO- d_6) δ ppm: 1.15–1.23 (2H, m, cyclopropyl-*H*), 1.29–1.34 (2H, m, cyclopropyl-*H*), 2.37 (3H, s, Ar- CH_3), 2.71–2.75 (4H, m, piperazinyl-*H*), 3.39–3.46 (4H, m, piperazinyl-*H*), 3.79–3.83 (3H, m, $N-CH_2$ and cyclopropyl-1*H*), 7.30 (2H, d, $J = 8$ Hz, Ar-*H*), 7.56 (1H, d, $J_{HFmeta} = 8$ Hz, C8-*H*), 7.75–7.82 (3H, m, =CH and Ar-*H*), 7.89–7.99 (2H, m, C5-*H* and =CH), 8.14 (2H, d, $J = 8$ Hz, Ar-*H*), 8.35 (2H, d, $J = 8$ Hz, Ar-*H*), 8.66 (1H, s, C2-*H*), 8.96 (1H, s, triazole *H*), 15.05 (1H, brs, COOH); ^{13}C NMR (100 MHz, $CDCl_3$) δ ppm: 8.20, 21.50, 35.26, 49.38, 50.46, 52.41, 52.83, 104.96, 108.27, 112.48 (C-5, d, $^2J_{Cortho} = 23$ Hz, C-F), 120.11, 120.47, 124.77, 128.60, 129.03, 129.79, 130.21, 131.94, 138.41, 139.07, 139.70, 141.55, 145.48, 145.89, 147.41, 148.32, 153.64 (C-6, d, $^1J_{CFipso} = 252$ Hz, C-F), 166.79, 177.06, 188.90; ESI-MS (m/z): Calcd. 632.25, found 655.40 $[M + Na]^+$. Anal. Calcd. For $C_{36}H_{33}FN_6O_4$: C, 68.34%; H, 5.26%; N, 13.28%. Found: C, 68.35%; H, 5.40%; N, 13.41%.

4.1.2.7. (E)-1-Cyclopropyl-6-fluoro-7-(4-((1-(4-(3-(4-methoxyphenyl)acryloyl)phenyl)-1H-1,2,3-triazol-4-yl)methyl)piperazin-1-yl)-4-oxo-1,4-dihydroquinoline-3-carboxylic acid 4g. Yellow powder; (0.47 g, 53.67% yield); mp: 254–257 °C; 1H NMR (400 MHz, DMSO- d_6) δ ppm: 1.18–1.24 (2H, m, cyclopropyl-*H*), 1.29–1.34 (2H, m, cyclopropyl-*H*), 2.70–2.75 (4H, m, piperazinyl-*H*), 3.35–3.40 (4H, m, piperazinyl-*H*), 3.76 (3H, s, OCH_3), 3.81–3.85 (3H, m, $N-CH_2$, cyclopropyl-*H*), 7.04 (2H, d, $J = 8$ Hz, Ar-*H*), 7.56 (1H, d, $J_{HFmeta} = 8$ Hz, C8-*H*), 7.77 (1H, d, $J_{trans} = 16$ Hz, =CH), 7.85–7.90 (4H, m, =CH, Ar-*H* and C5-*H*), 8.14 (2H, d, $J = 8$ Hz, Ar-*H*), 8.36 (2H, d, $J = 8$ Hz, Ar-*H*), 8.66 (1H, s, C2-*H*), 8.93 (1H, s, triazole-*H*), 15.16 (1H, brs, COOH); ^{13}C NMR (100 MHz, $CDCl_3$) δ ppm: 8.21, 35.25, 49.45, 52.47, 52.90, 55.45, 104.91, 108.30, 112.56 (C-5, d, $^2J_{Cortho} = 23$ Hz, C-F), 113.73, 114.58, 119.07, 120.07, 122.97, 127.38, 130.17, 130.42, 131.87, 138.58, 139.07, 139.58, 141.40, 145.69, 147.45, 153.66 (C-6, d,

$^1J_{CFipso} = 252$ Hz, C-F), 162.09, 166.88, 177.12, 188.83; ESI-MS (m/z): Calcd. 648.25, found 671.60 $[M + Na]^+$. Anal. Calcd. For $C_{36}H_{33}FN_6O_5$: C, 66.66%; H, 5.13%; N, 12.96%. Found: C, 66.39%; H, 5.36%; N, 13.18%.

4.1.2.8. (E)-1-cyclopropyl-7-(4-((1-(4-(3-(4-(dimethylamino)phenyl)acryloyl)phenyl)-1H-1,2,3-triazol-4-yl)methyl)piperazin-1-yl)-6-fluoro-4-oxo-1,4-dihydroquinoline-3-carboxylic acid 4h. Pale yellow powder; (0.39 g, 43.65% yield); mp: 177–179 °C; 1H NMR (400 MHz, DMSO- d_6) δ ppm: 1.17–1.21 (2H, m, cyclopropyl-*H*), 1.31–1.35 (2H, m, cyclopropyl-*H*), 2.74–2.78 (4H, m, piperazinyl-*H*), 3.04 (6H, s, $N(CH_3)_2$), 3.39–3.45 (4H, m, piperazinyl-*H*), 3.82–3.87 (3H, m, $N-CH_2$ and cyclopropyl-1*H*), 6.79 (2H, d, $J = 8$ Hz, Ar-*H*), 7.58–7.65 (2H, m, C8-*H* and =CH), 7.70–7.76 (3H, m, Ar-*H* and =CH), 7.91 (1H, d, $J_{HFortho} = 12$ Hz, C5-*H*), 8.10 (2H, d, $J = 8$ Hz, Ar-*H*), 8.30 (2H, d, $J = 8$ Hz, Ar-*H*), 8.67 (1H, s, C2-*H*), 8.83 (1H, s, triazole *H*), 15.07 (1H, brs, COOH); ^{13}C NMR (100 MHz, $CDCl_3$) δ ppm: 8.19, 35.28, 40.06, 49.57, 52.49, 52.97, 104.89, 108.15, 111.86, 112.38 (C-5, d, $^2J_{Cortho} = 23$ Hz, C-F), 116.02, 119.82, 119.97, 121.04, 122.34, 130.00, 130.65, 139.07, 139.13, 139.31, 144.77, 145.63, 145.72, 146.79, 147.37, 153.63 (C-6, d, $^1J_{CFipso} = 252$ Hz, C-F), 166.91, 177.06, 188.79; ESI-MS (m/z): Calcd. 661.28, found 684.50 $[M + Na]^+$. Anal. Calcd. For $C_{37}H_{36}FN_7O_4$: C, 67.16%; H, 5.48%; N, 14.82%. Found: C, 67.43%; H, 5.41%; N, 14.70%.

4.1.2.9. (E)-1-cyclopropyl-7-(4-((1-(4-(3-(3,4-dimethoxyphenyl)acryloyl)phenyl)-1H-1,2,3-triazol-4-yl)methyl)piperazin-1-yl)-6-fluoro-4-oxo-1,4-dihydroquinoline-3-carboxylic acid 4i. Yellow powder; (0.52 g, 56.77% yield); mp: 167–169 °C; IR (KBr) ν_{max} = broad band 3234–3067 cm^{-1} (OH of COOH), 1719 cm^{-1} (C=O of COOH), 1658 cm^{-1} (C=O of CH=CH-C=O) and 1625 (C=O of 4-keto gp of CP); 1H NMR (400 MHz, DMSO- d_6) δ ppm: 1.18–1.22 (2H, m, cyclopropyl-*H*), 1.29–1.32 (2H, m, cyclopropyl-*H*), 2.70–2.75 (4H, m, piperazinyl-*H*), 3.35–3.42 (4H, m, piperazinyl-*H*), 3.81–3.84 (6H, m, $N-CH_2$, cyclopropyl-*H*, OCH_3), 3.88 (3H, s, OCH_3), 7.04–7.08 (1H, m, Ar-*H*), 7.43–7.45 (1H, m, Ar-*H*), 7.55–7.60 (2H, m, Ar-*H* and C8-*H*), 7.76 (1H, d, $J_{trans} = 16$ Hz, =CH), 7.86–7.93 (2H, m, C5-*H* and =CH), 8.15 (2H, d, $J = 8$ Hz, Ar-*H*), 8.37 (2H, d, $J = 8$ Hz, Ar-*H*), 8.66 (1H, s, C2-*H*), 8.94 (1H, s, triazole-*H*), 15.17 (1H, brs, COOH); ^{13}C -NMR (100 MHz, $CDCl_3$) δ ppm: 8.20, 35.29, 49.48, 52.45, 52.89, 55.89, 56.06, 104.92, 108.13, 110.48, 111.32, 112.36 (C-5, d, $^2J_{Cortho} = 23$ Hz, C-F), 119.34, 120.07, 121.18, 123.45, 127.62, 130.19, 138.45, 139.06, 139.63, 145.58, 145.98, 147.38, 148.45, 149.44, 151.78, 151.91, 153.62 (C-6, d, $^1J_{CFipso} = 252$ Hz, C-F), 166.87, 177.02, 188.87; ESI-MS (m/z): Calcd. 678.26, found 701.50 $[M + Na]^+$. Anal. Calcd. For $C_{37}H_{35}FN_6O_6$: C, 65.48%; H, 5.20%; N, 12.38%. Found: C, 65.69%; H, 5.37%; N, 12.54%.

4.1.2.10. (E)-1-cyclopropyl-6-fluoro-4-oxo-7-(4-((1-(4-(3-(3,4,5-trimethoxyphenyl)acryloyl)phenyl)-1H-1,2,3-triazol-4-yl)methyl)piperazin-1-yl)-1,4-dihydroquinoline-3-carboxylic acid 4j. Yellow powder; (0.49 g, 51.21% yield); mp: 247–249 °C; 1H NMR (400 MHz, DMSO- d_6) δ ppm: 1.18–1.22 (2H, m, cyclopropyl-*H*), 1.27–1.32 (2H, m, cyclopropyl-*H*), 2.69–2.76 (4H, m, piperazinyl-*H*), 3.35–3.45 (4H, m, piperazinyl-*H*), 3.74 (3H, s, OCH_3), 3.78–3.85 (3H, m, $N-CH_2$, cyclopropyl-*H*), 3.89 (6H, s, 2X OCH_3), 7.26 (2H, s, Ar-*H*), 7.57 (1H, d, $J_{HFmeta} = 8$ Hz, C8-*H*), 7.75 (1H, d, $J_{trans} = 16$ Hz, =CH), 7.87 (1H, d, $J_{HFortho} = 12$ Hz, C5-*H*), 7.94 (1H, d, $J_{trans} = 16$ Hz, =CH), 8.15 (2H, d, $J = 8$ Hz, Ar-*H*), 8.37 (2H, d, $J = 8$ Hz, Ar-*H*), 8.65 (1H, s, C2-*H*), 8.94 (1H, s, triazole-*H*), 15.16 (1H, brs, COOH); ^{13}C NMR (100 MHz, $CDCl_3$) δ ppm: 8.22, 35.27, 49.15, 49.44, 52.42, 56.35, 61.00, 104.95, 106.11, 107.52, 108.23, 112.46 (C-5, d, $^2J_{Cortho} =$

23 Hz, C-F), 120.14, 120.76, 121.29, 130.02, 130.30, 137.38, 138.28, 139.07, 140.51, 141.07, 144.76, 146.00, 147.42, 153.21 (C-6, d, $^1J_{CF_{ipso}} = 252$ Hz, C-F), 153.62, 166.85, 177.07, 188.87; ESI-MS (m/z): Calcd. 707.28, found 730.26 $[M + Na]^+$. Anal. Calcd. For $C_{38}H_{37}FN_6O_7$: C, 64.40%; H, 5.26%; N, 11.86%. Found: C, 64.53%; H, 5.49%; N, 12.03%. HPLC analysis: 94.39%.

4.2. Biological investigations

4.2.1. Cell culture experiments and reagents

Colo-rectal cancer cell lines (Caco-2, HT29, and HCT116) were purchased from the American Type Culture Collection (Manassas, VA, USA). Cells were cultured and maintained in appropriate media supplemented with foetal bovine serum (10%) (Sigma-Aldrich, St. Louis, MO, USA), streptomycin (100 μ g/mL), and penicillin (100 U/mL) (Life Technologies) and incubated at 37 °C with CO₂ (5%). Ciprofloxacin derivatives were chemically synthesised (**4a-j**) while doxorubicin was obtained from Sigma-Aldrich. Analytical or cell culture grade chemicals were used throughout this study.

4.2.2. Proliferation assay

The method description for NCI anticancer screening is provided in detail in the standard NCI-60 testing protocol⁷².

4.2.3. 3-(4,5-dimethylthiazol-2-yl)-2,5-diphenyltetrazolium bromide (MTT) assay

The proliferation of colorectal cancer cells (HCT116, HT29 and Caco-2) was assessed using MTT assay as previously reported⁷³. Cells were treated with increasing concentrations of 1, 5, 10, 20, 40, 80 or 100 μ M of CP hybrids **4a-j**, doxorubicin, or DMSO. See Supplementary Appendix A.

4.2.4. Cytotoxicity assay with non-cancerous cells

To evaluate the selectivity and safety profile of the synthesised ciprofloxacin-chalcone hybrids, a cytotoxicity experiment was performed using a non-cancerous cell line. Briefly, Human Embryonic Kidney (HEK) 293 cells (ATCC, Manassas, VA, USA) were cultured in a Dulbecco's Modified Eagle Medium (DMEM) supplemented with 1 mM sodium pyruvate, 10 mM HEPES buffer solution, 2 mM GlutaMAX (Gibco, Grand Island, NY, USA), 50 μ g/mL gentamycin sulphate (Dubuque, IA, USA), and 10% foetal bovine serum (ThermoFisher Scientific, USA). Cells were seeded in 96-well plates and incubated overnight in a humidified atmosphere with 5% CO₂ at 37 °C. After 24 h, cells were treated with different concentrations (0.01–100 μ M) of ciprofloxacin-chalcone hybrids. Also, DMSO and doxorubicin were used as negative and positive controls, respectively. After 72 h, old medium containing treatments were removed, and fresh medium and MTS reagents (CellTiter 96® Aqueous One Solution Cell Proliferation Assay, Promega, Madison, WI, USA) were added. The plates were then incubated at 37 °C. After 2 h, the absorbance was measured at 490 nm using a Spectra Max plus 384 Microplate reader (Molecular Devices, Sunnyvale, CA, USA)⁷⁴. Also, before adding the MTS reagents, cells were examined under a cell imaging system (EVOS FL Digital Microscope using a 20x objective lens, total magnification = 200 \times).

4.2.5. Topoisomerase I inhibition assay

Two different assays were used to examine the inhibitory activity of IC₅₀ of the CP hybrids against Human topoisomerase I. Firstly;

Gel electrophoresis-based assay (DNA relaxation assay) was performed following the manufacturer's protocol (TG-1015, Topogen Inc., USA). Secondly, the inhibitory activity of compounds **4a**, **4b**, **4e**, **4i**, **4j**, and camptothecin to human topoisomerase I was analysed by Human DNA Topoisomerase I Assay Kit (ProFoldin, Hudson, MA, USA) with recombinant human DNA topoisomerase I (Sigma-Aldrich) according to the manufacturer's protocol.

4.2.6. Topoisomerase II inhibition assay

The inhibitory activity of the selected ciprofloxacin hybrids on human Top-II was tested using a Human Topoisomerase II assay kit (TG1001, Topogen Inc.). In this assay, 1% agarose gel was used, and the compounds were tested at two different concentrations, 10 and 100 μ M. Also, etoposide was used as a positive control in this experiment. The assay was performed according to the manufacturer's protocol. The image of the electrophoretic gel was captured using an imaging system (iBright-CL1500, Thermo Fisher Scientific).

4.2.7. Immunofluorescence microscopy

HCT116 cells were cultured and treated with the IC₅₀ of the potent compounds (**4a**, **4b**, **4e**, **4i**, and **4j**) or DMSO (control), fixed, permeabilized, and they were incubated with either γ H2AX or α -tubulin antibody as the reported procedure in the literature⁷⁵. Confocal images were captured using a Confocal Microscope with a 63X objective. All images were processed using ImageJ software. See Supplementary Appendix A.

4.2.8. Analysis of cell cycle distribution

The effects of the most potent CP hybrids; **4a**, **4b**, **4e**, **4i**, and **4j**, and assay controls; Doxorubicin, camptothecin, and etoposide on cell cycle progression were analysed through propidium iodide staining and subsequent flow cytometry according to the reported procedure⁷⁶. See Supplementary Appendix A.

4.2.9. Western blotting

Western blotting analysis for HCT116 cells was performed according to the reported procedure in the literature^{77–79} to determine the effects of CP hybrids; **4a**, **4b**, **4e**, **4i**, and **4j** on the expression of polymerised tubulin, γ H2AX, p-ATR, p-CHK1, and p-Cdc25C by using the appropriate antibody. See Supplementary Appendix A.

4.3. Docking studies

Compounds **4a**, **4b**, **4e**, **4i**, and **4j** were drawn and docked in the human Topo-I in complex with DNA and camptothecin (PDB ID: 1T8I) and in the human Top II in complex with DNA and Etoposide (PDB ID: **6ZY7**) using Molecular Operating Environment (MOE 2019.01) program as reported in the literature. See Supplementary Appendix A.

Disclosure statement

No potential conflict of interest was reported by the author(s).

Funding

Amer Ali Abd El-Hafeez was supported by an NIH-funded Cancer Therapeutics Training Program [CT2, T32 CA121938]. Pradipta

Ghosh was supported by the NIH [CA238042, CA100768 and CA160911]. The authors would like to thank the Deanship of Scientific Research at Umm Al-Qura University for supporting this work by Grant Code: [22UQU4290565DSR20].

ORCID

Samar H. Abbas  <http://orcid.org/0000-0002-9586-2644>

References

- Abdel-Aal MAA, Abdel-Aziz SA, Shaykoon MSA, Abuo-Rahma GE-DA. Towards anticancer fluoroquinolones: a review article. *Arch Pharm* 2019;352:e1800376.
- Kaushik CP, Sangwan J, Luxmi R, et al. Design, synthesis, anticancer and antioxidant activities of amide linked 1,4-disubstituted 1,2,3-triazoles. *J. Mol. Struct* 2021;1226:129255.
- Chekkara R, Gorla VR, Susithra E, et al. Design, synthesis and anticancer evaluation of 2-amino pyrimidine linked 7-azaindazole derivatives. *Chem. Data Collect* 2020;29:100513.
- El-Damasy AK, Haque MM, Park JW, et al. 2-Anilinoquinoline based arylamides as broad spectrum anticancer agents with B-RAFV600E/C-RAF kinase inhibitory effects: design, synthesis, *in vitro* cell-based and oncogenic kinase assessments. *Eur J Med Chem* 2020;208:112756.
- Baglini E, Salerno S, Barresi E, et al. Multiple topoisomerase I (Topol), topoisomerase II (Topoll) and Tyrosyl-DNA phosphodiesterase (TDP) inhibitors in the development of anticancer drugs. *Eur J Pharm Sci* 2021;156:105594.
- Xi Y, Xu P. Global colorectal cancer burden in 2020 and projections to 2040. *Transl Oncol* 2021;14:101174.
- Rodriguez-Wallberg KA. Principles of cancer treatment: impact on reproduction. *Adv Exp Med Biol* 2012;732:1–8.
- Dong Y, Hu H, Sun Y, et al. Design, synthesis and biological evaluation of novel c-Met/HDAC dual inhibitors. *Bioorg Med Chem Lett* 2020;30:127610.
- Chen J, Li D, Li W, et al. Design, synthesis and anticancer evaluation of acridine hydroxamic acid derivatives as dual Topo and HDAC inhibitors. *Bioorg Med Chem* 2018;26:3958–66.
- Zimmermann GR, Lehár J, Keith CT. Multi-target therapeutics: when the whole is greater than the sum of the parts. *Drug Discov Today* 2007;12:34–42.
- Anighoro A, Bajorath J, Rastelli G. Polypharmacology: challenges and opportunities in drug discovery. *J Med Chem* 2014;57:7874–87.
- Morphy R, Rankovic Z. Designed multiple ligands. An emerging drug discovery paradigm. *J Med Chem* 2005;48:6523–43.
- Bass AKA, El-Zoghbi MS, Nageeb E-SM, et al. Comprehensive review for anticancer hybridized multitargeting HDAC inhibitors. *Eur. J. Med. Chem* 2021; 209: 112904.
- Proschak E, Stark H, Merk D. Polypharmacology by design: a medicinal chemist's perspective on multitargeting compounds. *J Med Chem* 2019;62:420–44.
- Raghavendra NM, Pingili D, Kadasi S, et al. Dual or multi-targeting inhibitors: the next generation anticancer agents. *Eur J Med Chem* 2018;143:1277–300.
- Mohammed HHH, Abbas SH, Hayallah AM, et al. Novel urea linked ciprofloxacin-chalcone hybrids having antiproliferative topoisomerases I/II inhibitory activities and caspases-mediated apoptosis. *Bioorganic Chem* 2021;106:104422.
- Drlica K. Mechanism of fluoroquinolone action. *Curr Opin Microbiol* 1999;2:504–8.
- Shen LL, Baranowski J, Pernet AG. Mechanism of inhibition of DNA gyrase by quinolone antibacterials: specificity and cooperativity of drug binding to DNA. *Biochemistry* 1989;28:3879–85.
- Wang JC. Cellular roles of DNA topoisomerases: a molecular perspective. *Nat Rev Mol Cell Biol* 2002;3:430–40.
- Champoux JJ. DNA topoisomerases: structure, function, and mechanism. *Annu Rev Biochem* 2001;70:369–413.
- Abdel-Aziz M, Park S-E, Abuo-Rahma GE-DAA, et al. Novel N-4-piperazinyl-ciprofloxacin-chalcone hybrids: synthesis, physicochemical properties, anticancer and topoisomerase I and II inhibitory activity. *Eur J Med Chem* 2013;69:427–38.
- Azéma J, Guidetti B, Dewelle J, et al. 7-((4-Substituted)piperazin-1-yl) derivatives of ciprofloxacin: synthesis and *in vitro* biological evaluation as potential antitumor agents. *Bioorg Med Chem* 2009;17:5396–407.
- Sissi C, Palumbo M. The quinolone family: from antibacterial to anticancer agents. *Curr Med Chem Anticancer Agents* 2003;3:439–50.
- Reuveni D, Halperin D, Shalit I, et al. Quinolones as enhancers of camptothecin-induced cytotoxic and anti-topoisomerase I effects. *Biochem Pharmacol* 2008;75:1272–81.
- Yadav V, Varshney P, Sultana S, et al. Moxifloxacin and ciprofloxacin induces S-phase arrest and augments apoptotic effects of cisplatin in human pancreatic cancer cells via ERK activation. *BMC Cancer* 2015;15:581.
- Repositioning of fluoroquinolones from antibiotic to anticancer agents: an underestimated truth. *Biomed. Pharmacother* 2019;111:934–46.
- Mohammed HHH, Abuo-Rahma GE-DAA, Abbas SH, Abdelhafez E-SMN. Current trends and future directions of fluoroquinolones. *Curr Med Chem* 2019;26:3132–49.
- Ahadi H, Emami S. Modification of 7-piperazinylquinolone antibacterials to promising anticancer lead compounds: synthesis and *in vitro* studies. *Eur J Med Chem* 2020;187:111970.
- Yogeeswari P, Sriram D, Kavva R, Tiwari S. Synthesis and *in vitro* cytotoxicity evaluation of gatifloxacin Mannich bases. *Biomed Pharmacother* 2005;59:501–10.
- Nieto MJ, Alovero FL, Manzo RH, Mazzieri MR. Benzenesulfonamide analogs of fluoroquinolones. Antibacterial activity and QSAR studies. *Eur J Med Chem* 2005;40:361–9.
- Gootz TD, McGuirk PR, Moynihan MS, Haskell SL. Placement of alkyl substituents on the C-7 piperazine ring of fluoroquinolones: dramatic differential effects on mammalian topoisomerase II and DNA gyrase. *Antimicrob Agents Chemother* 1994;38:130–3.
- Foroumadi A, Emami S, Rajabalian S, et al. N-Substituted piperazinyl quinolones as potential cytotoxic agents: structure-activity relationships study. *Biomed Pharmacother* 2009; 63:216–20.
- Azéma J, Guidetti B, Korolyov A, et al. Synthesis of lipophilic dimeric C-7/C-7-linked ciprofloxacin and C-6/C-6-linked levofloxacin derivatives. Versatile *in vitro* biological evaluations of monomeric and dimeric fluoroquinolone derivatives as potential antitumor, antibacterial or antimycobacterial agents. *Eur J Med Chem* 2011;46:6025–38.
- Suresh N, Nagesh HN, Sekhar KVG, et al. Synthesis of novel ciprofloxacin analogues and evaluation of their anti-

- proliferative effect on human cancer cell lines. *Bioorg Med Chem Lett* 2013;23:6292–5.
35. Abdel-Aziz AA-M, El-Azab AS, Alanazi AM, et al. Synthesis and potential antitumor activity of 7-(4-substituted piperazin-1-yl)-4-oxoquinolines based on ciprofloxacin and norfloxacin scaffolds: *in silico* studies. *J Enzyme Inhib Med Chem* 2016;31:796–809.
 36. Mohammed HHH, Abd El-Hafeez AA, Abbas SH, et al. New antiproliferative 7-(4-(N-substituted carbamoylmethyl)piperazin-1-yl) derivatives of ciprofloxacin induce cell cycle arrest at G2/M phase. *Bioorg Med Chem* 2016;24:4636–46.
 37. Wang G, Liu W, Gong Z, et al. Design, synthesis, biological evaluation and molecular docking studies of new chalcone derivatives containing diaryl ether moiety as potential anticancer agents and tubulin polymerization inhibitors. *Bioorg Chem* 2020;95:103565.
 38. Zhang E-H, Wang R-F, Guo S-Z, Liu B. An update on antitumor activity of naturally occurring chalcones, *Evid Based Complement Alternat Med* 2013;2013:815621.
 39. Das M, Manna K. Chalcone scaffold in anticancer armamentarium: a molecular insight. *J Toxicol* 2016;2016:7651047.
 40. Mirzaei H, Shokrzadeh M, Modanloo M, et al. New indole-based chalconoids as tubulin-targeting antiproliferative agents. *Bioorg Chem* 2017;75:86–98.
 41. Yadav VR, Prasad S, Sung B, Aggarwal BB. The role of chalcones in suppression of NF- κ B-mediated inflammation and cancer. *Int Immunopharmacol* 2011;11:295–309.
 42. Singh P, Anand A, Kumar V. Recent developments in biological activities of chalcones: a mini review. *Eur J Med Chem* 2014;85:758–77.
 43. Batovska DI, Todorova IT. Trends in utilization of the pharmacological potential of chalcones. *Curr Clin Pharmacol* 2010;5:1–29.
 44. Bonandi E, Christodoulou MS, Fumagalli G, et al. The 1,2,3-triazole ring as a bioisostere in medicinal chemistry. *Drug Discov Today* 2017;22:1572–81.
 45. Xu Z, Zhao S-J, Liu Y. 1,2,3-Triazole-containing hybrids as potential anticancer agents: current developments, action mechanisms and structure-activity relationships. *Eur J Med Chem* 2019;183:111700.
 46. Akhtar J, Khan AA, Ali Z, et al. Structure-activity relationship (SAR) study and design strategies of nitrogen-containing heterocyclic moieties for their anticancer activities. *Eur J Med Chem* 2017;125:143–89.
 47. Lal K, Yadav P. Recent advancements in 1,4-disubstituted 1H-1,2,3-triazoles as potential anticancer agents. *Anticancer Agents Med Chem* 2018;18:21–37.
 48. Rashdan HRM, Gomha SM, El-Gendey MS, et al. Eco-friendly one-pot synthesis of some new pyrazolo[1,2-b]phthalazine-diones with antiproliferative efficacy on human hepatic cancer cell lines. *Green Chem. Lett. Rev* 2018;11:264–74.
 49. Gomha SM, Ahmed SA, Abdelhamid AO. Synthesis and Cytotoxicity evaluation of some novel thiazoles, thiadiazoles, and pyrido[2,3-d][1,2,4]triazolo[4,3-a]pyrimidin-5(1H)-ones incorporating triazole moiety. *Molecules* 2015;20:1357–76.
 50. Dheer D, Singh V, Shankar R. Medicinal attributes of 1,2,3-triazoles: current developments. *Bioorg Chem* 2017;71:30–54.
 51. Zhang B. Comprehensive review on the anti-bacterial activity of 1,2,3-triazole hybrids. *Eur J Med Chem* 2019;168:357–72.
 52. Victoria Castelli M, Gabriel Derita M, Noelí López S. Novel antifungal agents: a patent review (2013 –present). *Expert Opin Ther Pat* 2017;27:415–26.
 53. Emami S, Ghobadi E, Saednia S, Hashemi SM. Current advances of triazole alcohols derived from fluconazole: design, *in vitro* and *in silico* studies. *Eur J Med Chem* 2019;170:173–94.
 54. Tian Y, Liu Z, Liu J, et al. Targeting the entrance channel of NNIBP: discovery of diarylnicotinamide 1,4-disubstituted 1,2,3-triazoles as novel HIV-1 NNRTIs with high potency against wild-type and E138K mutant virus. *Eur J Med Chem* 2018;151:339–50.
 55. Kaoukabi H, Kabri Y, Curti C, et al. Dihydropyrimidinone/1,2,3-triazole hybrid molecules: synthesis and anti-varicella-zoster virus (VZV) evaluation. *Eur J Med Chem* 2018;155:772–81.
 56. Chu X-M, Wang C, Wang W-L, et al. Triazole derivatives and their antiplasmodial and antimalarial activities. *Eur J Med Chem* 2019;166:206–23.
 57. Kalaria PN, Karad SC, Raval DK. A review on diverse heterocyclic compounds as the privileged scaffolds in antimalarial drug discovery. *Eur J Med Chem* 2018;158:917–36.
 58. Keri RS, Patil SA, Budagumpi S, Nagaraja BM. Triazole: a promising antitubercular agent. *Chem Biol Drug Des* 2015;86:410–23.
 59. Zhang S, Xu Z, Gao C, et al. Triazole derivatives and their anti-tubercular activity. *Eur J Med Chem* 2017;138:501–13.
 60. M. M A. 1,2,3-Triazole hybrids as anticancer agents: a review. *Arch. Pharm* 2022;355:2100158.
 61. Oubella A, Bimoussa A, Oussidi AN, et al. New 1,2,3-triazoles from(R)-carvone: synthesis, DFTMechanistic study and *in vitro* cytotoxic evaluation. *Molecules* 2022;27:769.
 62. Ashour HF, Abou-zeid LA, El-Sayed MA-A, Selim KB. 1,2,3-Triazole-chalcone hybrids: synthesis, *in vitro* cytotoxic activity and mechanistic investigation of apoptosis induction in multiple myeloma RPMI-8226. *Eur J Med Chem* 2020;189:112062.
 63. Yan W, Xiangyu C, Ya L, et al. An orally antitumor chalcone hybrid inhibited HepG2 cells growth and migration as the tubulin binding agent. *Invest New Drugs* 2019;37:784–90.
 64. Gurrupu N, Kumar EP, Kolluri PK, et al. Synthesis, biological evaluation and molecular docking studies of novel 1,2,3-triazole tethered chalcone hybrids as potential anticancer agents. *J. Mol. Struct* 2020;1217:128356.
 65. Rahulan KM, Balamurugan S, Meena KS, et al. Synthesis and nonlinear optical absorption of novel chalcone derivative compounds. *Opt. Laser Technol* 2014;56:142–5.
 66. Balamurugan S, Nithyanandan S, Selvarasu C, et al. Photophysical and photochemical investigations on triazole ring linked chalcone containing polymethacrylates. *Polymer* 2012;53:4104–11.
 67. McPherson JC, Runner R, Buxton TB, et al. Synthesis of osteotropic hydroxybisphosphonate derivatives of fluoroquinolone antibacterials. *Eur J Med Chem* 2012;47:615–8.
 68. Keepers YP, Pizao PE, Peters GJ, et al. Comparison of the sulforhodamine B protein and tetrazolium (MTT) assays for *in vitro* chemosensitivity testing. *Eur J Cancer Clin Oncol* 1991;27:897–900.
 69. Perez RP, Godwin AK, Handel LM, Hamilton TC. A comparison of clonogenic, microtetrazolium and sulforhodamine B assays for determination of cisplatin cytotoxicity in human ovarian carcinoma cell lines. *Eur J Cancer* 1993;29:395–9.
 70. Iqbal H, Prabhakar V, Sangith A, et al. Synthesis, anti-inflammatory and antioxidant activity of ring-A-monosubstituted chalcone derivatives. *Med. Chem. Res* 2014;23:4383–94.

71. Worrell BT, Malik JA, Fokin VV. Direct evidence of a dinuclear copper intermediate in Cu(I)-catalyzed azide-alkyne cycloadditions. *Science* 2013;340:457–60.
72. <https://dtp.cancer.gov>.
73. Marwa Ali A, Fathi AA, Abd El-Hafeez DA, Abbas SH, Montano MM, Mohamed Abdel-Aziz, 1,3,4-oxadiazole/chalcone hybrids: Design, synthesis, and inhibition of leukemia cell growth and EGFR, Src, IL-6 and STAT3 activities. *Bioorganic Chem* 2019;84:153–60.
74. Mekkawy AI, Naguib YW, Alhaj-Suliman SO, et al. Paclitaxel anti-cancer activity is enhanced by the MEK 1/2 inhibitor PD98059 in vitro and by PD98059-loaded nanoparticles in BRAFV600E melanoma-bearing mice. *Int J Pharm* 2021;606:120876.
75. Popp HD, Brend S, Hofmann W-K, Fabarius A. Immunofluorescence microscopy of γ H2AX and 53BP1 for analyzing the formation and repair of DNA double-strand breaks. *J Vis Exp* 2017;129:e56617.
76. Ryu MJ, Chung HS. [10]-Gingerol induces mitochondrial apoptosis through activation of MAPK pathway in HCT116 human colon cancer cells. *In Vitro Cell Dev Biol Anim* 2015;51:92–101.
77. Ahmed FF, Abd El-Hafeez AA, Abbas SH, et al. New 1,2,4-triazole-chalcone hybrids induce caspase-3 dependent apoptosis in A549 human lung adenocarcinoma cells. *Eur J Med Chem* 2018;151:705–22.
78. P. Giannakakou DL, Sackett Y-K, Kang Z, et al. Paclitaxel-resistant human ovarian cancer cells have mutant beta-tubulins that exhibit impaired paclitaxel-driven polymerization. *J Biol Chem* 1997;272:17118–25.
79. Sinha S, Field JJ, Miller JH. Use of substitute Nonidet P-40 nonionic detergents in intracellular tubulin polymerization assays for screening of microtubule targeting agents. *Biochem Cell Biol* 2017;95:379–84.